Universiteit Utrecht

Point defects in crystals of point Yukawa particles

Faculty of Science
Bachelor Thesis

Rinske Alkemade
Physics and Astronomy

Supervisors:

Dr. Laura Filion
Debye Institute

Dr. Berend van der Meer
Debye Institute

16-1-2019

Cover Design: Rinske Alkemade

Abstract

We studied vacancies and interstitials in both body centered cubic (BCC) and face centered cubic (FCC) crystals of point Yukawa particles. To this end, we used Monte Carlo simulations combined with various types of thermodynamic integration and Wang Landau biasing. With these methods we determined the concentration of both defects at the phase boundaries of the system and looked at how the defects manifest themselves in the crystals. We found that the concentration of vacancies is around the same order of magnitude as the concentration of interstitials along both the fluid-BCC and the BCC-FCC/fluid-FCC phase boundary. Furthermore we found that at the BCC-FCC phase boundary the concentration of vacancies in a BCC crystal is between 2 or 3 orders of magnitude higher than the concentration in an FCC crystal. We studied and explained this concentration difference by looking at how the particles in the two crystals redistributed due to the presence of a vacancy. In the case of an interstitial we saw that the crystal structures of both FCC and BCC crystals are distorted along all the directions of the nearest neighbors of the interstitial. In the case of a BCC crystal this distortion might be indicating a crowdion, however more research is needed to draw firm conclusions.

Contents

Chapter 1

Overview of thesis project

From a theoretical point of view, a crystal is a perfectly ordered arrangement of particles. In practice, however, imperfections, so called *defects*, disturb this perfect ordering. The variety of possible defects is enormous and we usually classify them in three categories: point defects, line defects and planar defects. Point defects include for example *interstitials* and *vacancies*, denoting respectively a lattice site with an extra particle and a lattice site without a particle. An example of a line defect is an *edge dislocation*, which is an extra half-plane of particles in a lattice. Finally planar defects include for instance a *grain boundary*, where the crystal has regions of differently oriented crystallites. Cartoons of some defects are displayed in Figure 1.1. Defects occur naturally in materials: it can be shown that at any finite temperature, the equilibrium concentration of vacancies and interstitials is always finite [1]. However, the concentration of defects is generally very low.

Although their concentration is low, the influence that defects can have on crystalline properties can be huge. Point defects for example can strengthen metals, and grain boundaries in specific cases can make it possible for a material to be elongated extraordinarily [1]. Furthermore defects influence thermodynamical, mechanical and dynamical properties of materials. Because of the influence defects have, we sometimes purposely create them in crystalline structures, establishing materials that have useful properties. An example of this is the process of strengthening steel. By heating steel, one creates defects, resulting in a stronger material [2].

Defect concentration

Although it is clear that in real systems the influence of defects can be potentially very large, in simulations and numerical studies it is often assumed that their existence can be ignored. In some systems or for some purposes this assumption is indeed valid; take for example the very basic single component hard-sphere model. Here, all particles are assumed to be marble-like, meaning that the potential between particles is zero, except for when they try to overlap, which results in an infinitely high potential at contact. Bennet and Alder have looked at such a system and have obtained the vacancy concentration [3]. They found that in a three-dimensional face centered cubic crystal at melting point the equilibrium vacancy concentration is on the order of 10^{-4} [3]. Although this concentration is large enough to have a small influence on the free energy, overall the assumption that the vacancies can be ignored is quite accurate. Pronk and Frenkel subsequently looked at the interstitial concentration and found it to be even smaller, on the order of 10^{-8} [4].

However, the assumption to ignore defects is not always justifiable. This becomes clear if we look, for example, at a hard-sphere model with some slight alterations. In Ref. [5], for instance, the researchers looked at a hard-cube system, where the particles are cubical instead of spherical. They investigated the vacancy concentration and found a really surprising result: for the first-order phase transition between a fluid and a simple cubic phase, the vacancy concentration is on the order of 6 % [5]. A high number that, contrary to the the spherical

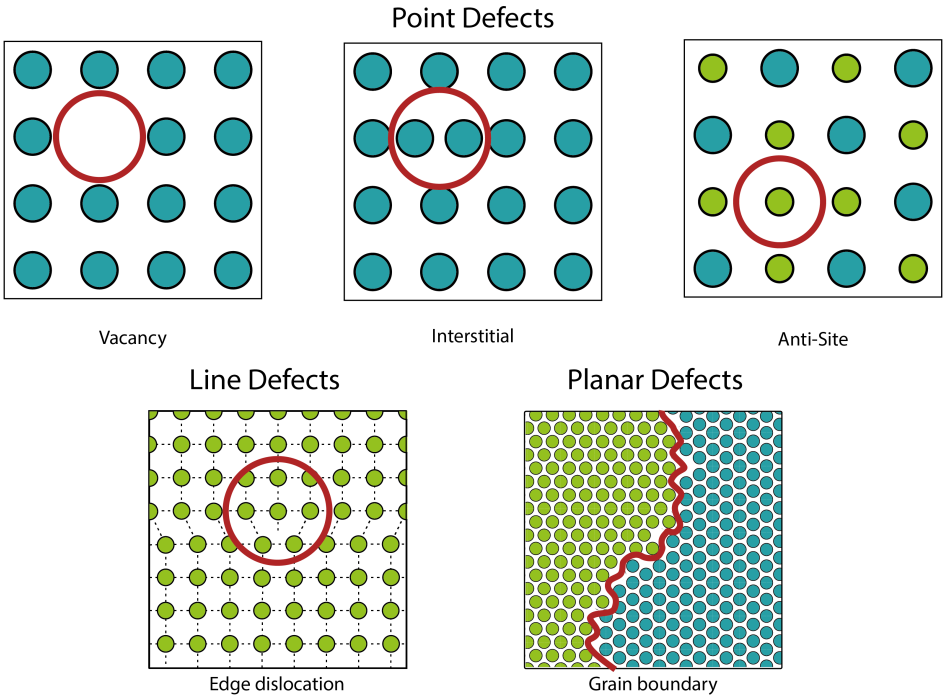

Figure 1.1: *Cartoon of different crystalline defects. The red circles/curve indicate the position of the defect.*

case, can definitely not be ignored.

Another system where defects cannot be ignored is a binary hard-sphere model, which consists of two species of hard spheres with different radii. Van Der Meer and Filion considered anti-site defects for such a system [6]. These defects occur when two particles of different species switch position in the crystalline ordering. For a ratio between the two particle radii of 0.82, they found that up to 2% of the larger particles was substituted by a smaller particle in equilibrium [6]. This is a very big concentration that results in a significant change in the phase diagram of the binary mixture.

From these examples it thus becomes clear that the concentration of defects hugely depends on the specific system and the phase it is in.

Manifestation of Defects in Crystals

Apart from the topic of defect concentrations, another very interesting subject is how defects manifest themselves in crystals. It turns out that defects change the arrangement of the crystal and sometimes even interact with other defects, giving rise to interesting structures such as defect strings [5].

Research on the way interstitials and vacancies manifest themselves has been conducted for three-dimensional crystals. A very interesting result of this research is the forming of a so called *crowdion* in a BCC lattice. A crowdion is, as stated in Ref. [7], the extended distortion of the crystal in the 111 direction due to a single interstitial. This means that only along this direction particles are pushed away from the interstitial; the rest of the crystal is unaffected.

Aim of this thesis

We may conclude that the field of crystalline defects yields interesting and sometimes even intriguing results. It is very worthwhile to gain more understanding on how defects are formed, how they behave and how often they occur in specific systems.

In this thesis we will consider vacancies and interstitials in a system of charged colloidal particles dispersed in a suspension of counter-charged ions. Colloidal particles, or colloids for short, are particles that have typical dimensions between $1nm$ and $1\mu m$, which means that they are much larger than single atoms and molecules. In a colloidal system, the colloids, dispersed in a suspension containing much smaller particles, can self assemble. Although these colloidal systems are in general quite complicated, it is often possible to use relatively simple models to describe them, such as the point Yukawa potential that we will use in this thesis. This potential, that is one of the simplest extensions of the hard-sphere model, basically describes a screened Coulomb interaction.

The aim of this thesis is to compute the vacancy and interstitial concentration along the phase boundaries of the point Yukawa system and to get a basic picture of how these defects alter the crystalline structures. In Chapter 2 we will briefly discuss some theory behind the Yukawa potential and point defects. Thereafter, in Chapter 3 we will discuss the general methods used in this thesis, which we will then specify in Chapter 4 for computing the free energies required to obtain the defect concentration. We conclude with the results and corresponding discussions and conclusions in Chapters 5 and 6.

Chapter 2

Yukawa potential and point defects

In this chapter we will discuss the Yukawa potential of soft-core particles. Furthermore we will take a closer look at the point defects of interest and determine an expression for the concentration of these defects in a crystalline system. It is by no means the purpose of this chapter to give the reader an extensive discussion of these theories. The goal is mainly to indicate which theories are used in this thesis and to give a quick overview of them.

2.1 Yukawa potential

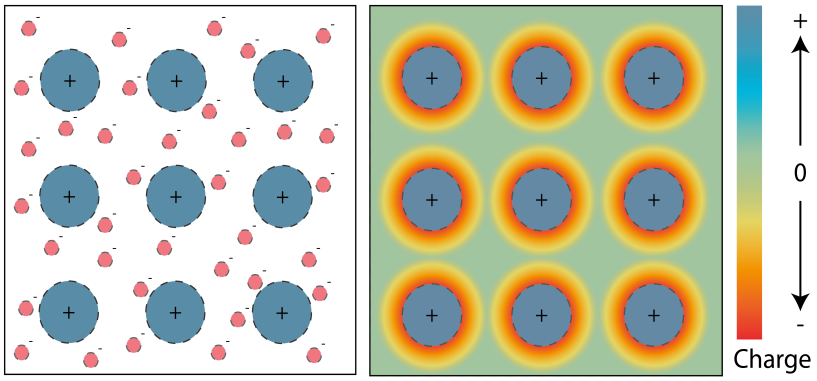

Figure 2.1: *Cartoon of a Yukawa system. In the left figure the system consists of colloids (indicated as blue) and individual ions (indicated as red). The colloids and ions, although being soft cored, are displayed as having a finite radius to indicate that the charge of the colloids is bigger than the charge of the ions. In the right figure the solvent is modeled as a continuum with a dielectric constant (where the exact distribution of course depends on the specifics of the system), instead of being viewed as containing individual ions.*

Sometimes when colloids are placed in a solvent, they lose ions, also called *counter-ions* to the solvent due to chemical reactions. The colloid is then left with a charge opposite to the released ions. In addition to the released counter-ions, the solvent itself can also contain *added salt*, consisting of counter-ions and *co-ions* (having the same charge as the colloids). Due to electrodynamics, the density of the counter-charged ions will be the highest in a band around the colloids. Because of this band, the interactions between colloids become screened.

Solving the dynamics of this system is very complicated due to the fact both the colloids and the individual ions need to be taken into account in the computation. In order to simplify the system, we therefore treat the solvent as a smooth continuum with a dielectric constant, rather than treating the ions as point particles [8]. There are a lot of materials, for example dusty plasmas, whose structures can be very well described using this simplification. In this case, as mentioned earlier we furthermore assume the colloids to have no radius, implying that their interactions are soft core.

Both the real, physical system and the Yukawa model are displayed in Figure 2.1. To obtain the potential for the system with the assumptions mentioned above, one has to solve the so called *linearized Poisson-Boltzmann equations* [9]. We will not state the derivation here, but just present the results. The effective potential, also called the *Yukawa potential*, for the colloidal particles in the system described above is given by [10]

$$\phi(r) = \frac{Q^2}{4\pi\epsilon_0 r} e^{-\kappa_D r} = \frac{\epsilon}{r} e^{-\kappa_D r}, \tag{2.1}$$

where Q is the charge of a colloid, ϵ_0 is the permittivity in vacuum, ϵ is the interaction energy defined by $\frac{Q^2}{4\pi\epsilon_0}$, κ_D is the screening length of the system and r is the radial distance between the particles. Physically, we can regard this potential as a normal Coulomb potential, indicated by the $\frac{Q^2}{4\pi\epsilon_0 r}$ term, multiplied with an exponentially decaying term, which accounts for the screening that colloidal particles feel due to the oppositely charged solvent surrounding them.

Looking at Equation (2.1), one might expect that the phase behavior of the system depends

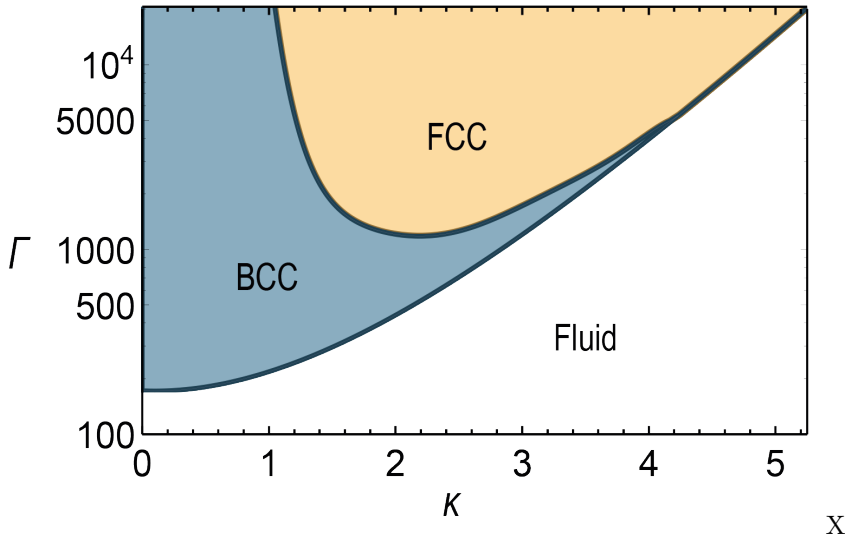

Figure 2.2: *Phase diagram of Yukawa systems in the* (κ, Γ) *plane[10][11].*

on three parameters: the number density ρ (which has an influence on the typical distance between colloids), the screening length κ_D and the interaction energy ϵ. However, because we look at point particles, the density is not an independent parameter and we can, by introducing two specific dimensionless parameters, κ and Γ, reduce the number of independent parameters to two. We define κ and Γ as [10]:

$$\Gamma = \frac{\epsilon}{a k_B T} \text{ and } \kappa = a\kappa_D,$$

where $a = \left(\frac{4\pi N}{3V}\right)^{-\frac{1}{3}}$ is the Wigner Seitz radius. This radius is defined as the radius of the spherical volume equal to the Wigner Seitz volume. Rewriting Equation (2.1) in terms of Γ, κ and a, we find:

$$\frac{\phi(r)}{k_B T} = \Gamma \left(\frac{a}{r}\right) e^{-\kappa\left(\frac{r}{a}\right)}. \tag{2.2}$$

Here we have introduced the reduced length scale $\frac{r}{a}$, the temperature T and the Boltzmann constant k_B. Using these dimensionless parameters has the advantage that instead of a 3-dimensional phase diagram, the phase behavior can completely be summarized in a 2-dimensional phase diagram. This 2-dimensional phase diagram is shown in Figure 2.2 [10][11]. As we can see it consists of three phases: a fluid, an face centered cubic (FCC) crystal and a body centered cubic (BCC) crystal. Both crystals are displayed in Figure 2.3. Since we are interested in the concentration of defects at the phase boundaries of a Yukawa system, this means that we will consider both FCC and BCC crystals in this thesis.

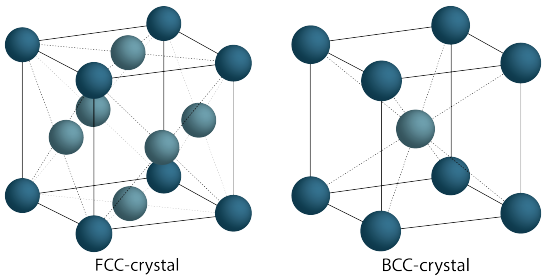

Figure 2.3: *Crystal structures of FCC and BCC crystals*

Later we will also need the force between particles due to the Yukawa potential. Using the fact that $\vec{F} = -\nabla\phi(\vec{r})$, this force is given by

$$\frac{\vec{F}(r)}{k_B T} = \left[\Gamma \left(\frac{a}{r^2} + \frac{\kappa}{r}\right) e^{-\kappa\left(\frac{r}{a}\right)}\right] \hat{r}, \tag{2.3}$$

where $\hat{r}$ is the unit vector in radial direction. As we can see, this force only has a radial component.

2.2 Crystal structures and point defects

In this section we will take a closer look at the two point defects considered in this thesis, namely interstitials and vacancies, and deduce expressions for their associated free energies and concentrations. Both point defects are schematically displayed in Figure 2.4. As we see, a vacancy indicates that there is a lattice site without a particle, whereas in the case of an interstitial there is a lattice site that contains two particles.

Before we go to the real calculations, we first briefly discuss the physics that explains why point defects occur in crystals. As stated in Chapter 1, the concentration of vacancies and interstitials is finite for all finite temperatures. This might seem counter intuitive as creating a defect increases the potential energy U. However, while it increases U, it also increases the entropy, S. This increase of S explains the occurrence of defects: in the Helmholtz free energy, $F = U - TS$, the terms U and S have a opposite sign, implying that defects can, in principle, also lower the free energy. One can show that for $T > 0$ the lowest free energy is indeed always found for a finite concentration of defects [1].

2.2.1 Concentrations of vacancies and interstitials in crystals

The method of deriving the free energy and concentration is almost the same for vacancies and interstitials. In this section we will therefore focus our attention on the expressions concerning vacancies and just state the results for interstitials at the end.

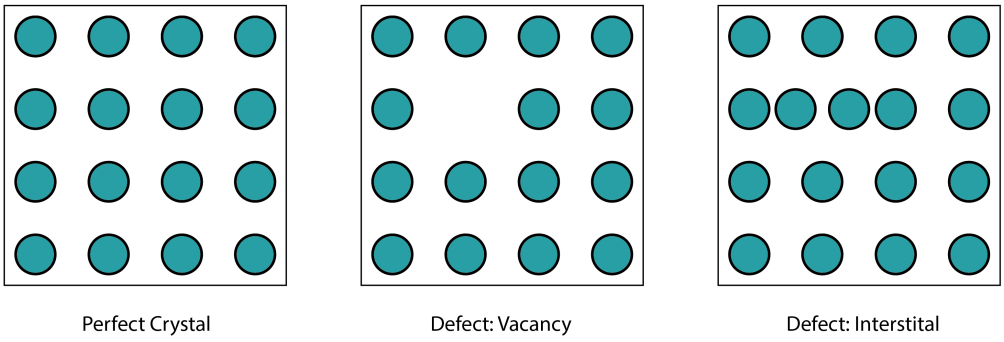

Figure 2.4: *Cartoon of defects in a crystal*

To find the equilibrium concentration of vacancies we need to find the concentration for which the system is in an energy minimum. It turns out that the expression for this concentration becomes quite elegant if we obtain it using the Gibbs free energy. Because we cannot express the Gibbs free energy of this crystal directly, we first express the Helmholtz free energy of the system and then transfer to the Gibbs free energy.

For the free-energy calculation we make two assumptions. First of all we assume the vacancies to be non-interacting and secondly we assume the pressure of a crystal with vacancies, P^{vac}, to be equal to the pressure of a perfect crystal P^{perfect}. Both assumptions are expected to hold as long as the concentration of vacancies is sufficiently low (something we do expect) and they simplify the calculations considerably.

We first calculate the Helmholtz free energy of a system with vacancies and than switch to the Gibbs free energy. Assume that the Helmholtz free energy of a perfect crystal is given by $F^{\text{perfect}}(N, V, T)$ with V the volume, T the temperature and N the number of particles. We denote the number of lattice sites by M and number of vacancies by N^{vac}. For a perfect crystal M is of course equal to N, but for a crystal with vacancies $M > N$ and N^{vac} is given by $M - N$. We express the free energy associated with one vacancy[1] by $f^{\text{vac}}(\rho_m, T)$, with $\rho_m = M/V$ the density of lattice sites.

Keeping the assumptions mentioned above in mind, we can define the Helmholtz free energy of a crystal with vacancies. The total free energy of our system is now given by the free energy of a perfect crystal, $F^{\text{perfect}}(N, V, T)$, plus the free energy associated with the vacancies only, $F^{\text{V}}(N, V, T)$. We can write this last term as $F^{\text{V}} = -k_B T \log(Z^{\text{vac}})$, with Z^{vac} the partition function associated with the vacancies. We want to express this Z^{vac} in terms of quantities we know.

The partition function Z^{vac} is in a canonical system defined as the sum of the Boltzmann weights over all possible micro states. In this case the number of micro states is determined by the number of ways the vacancies can distribute themselves over the crystal. All micro states have an energy of $N^{\text{vac}} f^{\text{vac}}(\rho_M, T)$, which means that,

$$Z^{\text{vac}} = \sum_{\text{micro states}} e^{-\beta N^{\text{vac}} f^{\text{vac}}} = \binom{M}{N^{\text{vac}}} e^{-\beta N^{\text{vac}} f^{\text{vac}}}. \tag{2.4}$$

Working out the expression for $F^{\text{V}}(N, V, T)$, using Equation (2.4), on finds that the Helmholtz

[1] This is the energy needed to change a perfect crystal into a crystal containing one.

free energy, F^{vac}, of a crystal with N^{vac} vacancies is given by

$$\beta F^{\text{vac}}(N,V,T) = \beta M f^{\text{perfect}}(N,V,T) + \beta(M-N)f^{\text{vac}} + N\log\frac{N}{M} + (M-N)\log\frac{M-N}{M}, \tag{2.5}$$

where $f^{\text{perfect}}(N,V,T) \equiv F^{\text{perfect}}(N,V,T)/M$ and where we have replaced N^{vac} by $M-N$. We can understand this expression as follows: the first term is the energy associated with the perfect crystal, the second term is the energy associated with removing N^{vac} particles out of the system and the last terms are associated with the combinatorial terms due to the possible positions of the vacancies.

Now that we have an expression for the Helmholtz free energy of a crystal with vacancies, we will transform to the Gibbs free energy. To do so we use two of the definitions of G:

$$\beta G = \beta F + \beta PV = \beta\mu N,$$

where μ is the chemical potential of a particle. Using these definitions, we can write the Gibbs free energy of a perfect crystal, $G^{\text{perfect}}(N,P,T)$ as

$$\beta G^{\text{perfect}}(N,P,T) = \beta M f^{\text{perfect}}(N,V,T) + \beta PV = \beta\mu^{\text{perfect}}(P,T)M. \tag{2.6}$$

To obtain subsequently the Gibbs free energy, G^{vac}, for a system with vacancies, we use the definition of the Gibbs free energy together with Equations (2.5) and (2.6) and the assumption that the pressure does not change when vacancies arise. With a bit of rearranging, we find

$$\begin{aligned}\beta G^{\text{vac}} &= \beta F^{\text{vac}}(N,V,T) + \beta PV,\\ &= \beta M\mu^{\text{perfect}}(P,T) + \beta(M-N)f^{\text{vac}}(\rho_M,T) + N\log\frac{N}{M} + (M-N)\log\frac{M-N}{M},\\ &= \beta N\mu^{\text{perfect}}(P,T) + \beta(M-N)\mu^{\text{vac}}(P,T) + N\log\frac{N}{M} + (M-N)\log\frac{M-N}{M},\end{aligned} \tag{2.7}$$

where we have defined $\mu^{\text{vac}} \equiv f^{\text{vac}}(\rho_M,T) + \mu^{\text{perfect}}(P,T)$.

Using the Gibbs free energy of Equation (2.7), we can now obtain the equilibrium concentration of vacancies denoted by $\left\langle\frac{M-N}{N}\right\rangle$. To find this concentration we take the derivative of Equation (2.7) with respect to the number of lattice sites M and set it to zero. We then obtain:

$$\langle n_{\text{vac}}\rangle \equiv \left\langle\frac{M-N}{N}\right\rangle = \exp[-\beta\mu^{\text{vac}}], \tag{2.8}$$

We can understand this expression as follows: to obtain a vacancy we first need to remove a particle from the system, increasing[2] the energy of the system by $f^{\text{vac}}(\rho_M,T)$. That particle then needs to be put away in an external, similar system, increasing the energy of that system with $\mu^{\text{perfect}}(P,T)$. Those two terms combined give the μ^{vac} term.

Equilibrium concentration of vacancies

The derivation for the equilibrium concentration of interstitials is almost the same, as stated in the beginning of the chapter. Defining $f^{\text{int}}(\rho_M,T)$ as the free energy associated with an interstitial and using the same procedure as described above, we find that the equilibrium concentration of interstitials is given by:

$$\langle n_{\text{int}}\rangle \equiv \left\langle\frac{N-M}{N}\right\rangle = \exp[-\beta\mu^{\text{int}}], \tag{2.9}$$

with $\mu^{\text{int}} = f^{\text{int}}(\rho_M,T) - \mu^{\text{perfect}}(P,T)$. The minus sign in front of $\mu^{\text{perfect}}(P,T)$ occurs because in this case the interstitial particle is obtained from the external system, lowering the energy of that system with $\mu^{\text{perfect}}(P,T)$.

[2]Note that $f^{\text{vac}}(\rho_M,T)$ can be negative, which means that it can actually lower the free energy of the system.

2.2.2 Parameters to obtain

Now that we have found expressions for the concentration of vacancies and interstitials, we can write down the quantities needed in order to evaluate these expressions. Using Equations (2.8) and (2.9), it becomes clear that we have to obtain values for $\mu^{\text{perfect}}(P,T)$, $f^{\text{int}}(\rho_M,T)$ and $f^{\text{vac}}(\rho_M,T)$. As said before, we will find these values by performing computer simulations. In Chapter 4 we will take a closer look at the specific simulations we need to obtain these free energies. However we first discuss some general background on simulations and free-energy calculations in Chapter 3.

Chapter 3

Methods

In this chapter we will discuss different simulation methods and other techniques that we will use for our simulations. In Section 3.1 we look at Monte Carlo simulations, in Sections 3.2 and 3.3 we discuss respectively thermodynamic integration and Wang Landau biasing. We then end the chapter with Section 3.4 where we discuss the general characteristics of the simulations used.

3.1 Monte Carlo simulation

In this thesis we will use Monte Carlo (MC) simulations as the basis for all our simulations. Although MC simulations are used in a very wide range of applications, we will in this thesis focus only on Monte Carlo simulations in thermodynamic ensembles [12]. In this setting MC simulations are very useful to compute ensemble averages. Normally an ensemble average, say for example $\langle A \rangle$, would be given by

$$\langle A \rangle = \lim_{n \to \infty} \frac{\sum_{i=1}^{n} f_c(\vec{r}_i^N) A(\vec{r}_i^N)}{n},$$

where $f_c(\vec{r}_i^N)$ is the Boltzmann weight of configuration i, $A(\vec{r}_i^N)$ is the value of the quantity A in configuration i and n indicates the number of generated configurations. A Monte Carlo simulation generates completely random configurations, and then accepts or rejects them depending on how likely the configuration is energetically. This means that states with a high energy, or consequently a low Boltzmann weight, will be visited less often than lower energy configurations. Using this procedure of generating configurations, the ensemble average is then simply be computed by

$$\langle A \rangle = \lim_{n \to \infty} \frac{\sum_{i=1}^{n} A(\vec{r}_i^N)}{n}.$$

Of course we can never have infinitely many steps, but for a large n, the result will still be very accurate. We use Monte Carlo simulations in this thesis because they are quite easy to program and it is simple to extend them to different ensembles.

Move acceptance

In our application of Monte Carlo simulations, configurations are are generated according to their Boltzmann weight. We will now look at how these configurations are obtained in more detail.

To ensure that the Monte Carlo simulation generates configurations according to their Boltzmann weights, the rule to accept a trial configuration must satisfy two conditions. First of all, it must be in principle possible to visit all configurations. The second condition is the so-called *balance condition*, which states that in equilibrium the probability of going into a

certain configuration must be equal to the probability of leaving that configuration. It is common, however, to impose an even stronger condition than the balance condition, namely the *detailed balance condition*. This condition states that the number of accepted moves[1] going from state o to state n must be equal to the number of accepted moves going from state n to state o, where n and o are random configurations. The mathematical expression for this condition is given by

$$f_c(\vec{r_o}^N)\pi(o \to n) = f_c(\vec{r_n}^N)\pi(n \to o), \tag{3.1}$$

where $f_c(\vec{r_i}^N)$ is the probability of being in state i (which is equal to the Boltzmann weight) and $\pi(i \to j)$, the transition matrix, is the probability of going from state i to state j. The aim is now to find an *acceptance rule*, satisfying both conditions mentioned above, that states whether to accept or reject a randomly generated move. To obtain this rule, we take a closer look at the transition matrix.

This transition matrix can be broken into two terms, by writing it as

$$\pi(0 \to n) = \alpha(0 \to n)acc(0 \to n). \tag{3.2}$$

In this equation $\alpha(o \to n)$ indicates the probability of trying a move and $acc(o \to n)$ indicates probability of accepting that move. This last term, $acc(o \to n)$, is the term we are interested in for it holds the information whether to accept a move or not. We choose $\alpha(o \to n)$ to be equal to $\alpha(n \to 0)$, which means that trying a move is symmetrical. Using Equations (3.1) and (3.2), we then find

$$\frac{acc(o \to n)}{acc(n \to o)} = \frac{f_c(\vec{r_n}^N)}{f_c(\vec{r_o}^N)} \tag{3.3}$$

Though we are free to choose any expression for $acc(o \to n)$ that satisfies Equation (3.3), the usual choice is [12]

$$acc(o \to n) = \min\left(\frac{f_c(\vec{r_n}^N)}{f_c(\vec{r_o}^N)}, 1\right). \tag{3.4}$$

Different acceptance rules

The explicit form of Equation (3.4) depends on the sort of move the Monte Carlo simulation tries to make. In this thesis we will do simulations in an NVT-ensemble, however we check if the simulation of this ensemble works correctly by using an NPT-ensemble. This means that we need to define the sort of MC moves attempted in both ensembles and then find the corresponding acceptance rules for these moves.

During a Monte Carlo simulation of an NVT-ensemble, every step an attempt is made to move a particle by a distance $\delta\mathbf{r}$. Each component of this vector, denoted by δr_i, satisfies $|\delta r_i| \leq \delta r_{\max}$ for a defined value of $\delta r_{\max}$. In an NPT-ensemble, in addition to the attempt of moving particles, there is another move that tries to change the volume by an amount δV. Again δV satisfies $|\delta V| \leq \delta V_{\max}$ for a defined $\delta V_{\max}$. We will discuss later how to find $\delta V_{\max}$ and $\delta r_{\max}$

As said before, the concrete expression of the acceptance rule defined in Equation 3.4 changes depending on the type of move. We will not go through the entire computations of these rules, but just state the results here. For a particle move, the acceptance rule is given by Ref. [12]

$$acc(o \to n) = \min[\ \exp\left[-(\beta(U(\mathbf{r}_n^N))) - \beta(U(\mathbf{r}_0^N))\right], 1], \tag{3.5}$$

[1] We will later go into detail about what trying a move exactly means.

while for a volume move it is given by

$$acc(o \to n) = \min[\ \exp[-(\beta(U(\mathbf{r}_n^N, V_n))) - \beta(U(\mathbf{r}_o^N, V_o)) + P(V_n - V_o) + N\beta^{-1} \log\left(\frac{V_n}{V_o}\right), 1]. \tag{3.6}$$

Here V_o is the volume of the simulation box in state o, V_n is the volume of the simulation box in state n, β is the Boltzmann weight defined by $\frac{1}{k_B T}$, $U(\mathbf{r}_i^N)$ is the potential energy of state i, P is the pressure and N is the total number of particles. In an NVT ensemble the acceptance rule thus only depends on the positions of the particles, whereas in an NPT ensemble the rules depend on the particle positions as well as the volume.

Acceptance ratio and finding $\delta\mathbf{r}_{\max}$ and $\delta\mathbf{V}_{\max}$

The last thing we need to discuss is how to define the values of $\delta r_{\max}$ and $\delta V_{\max}$. Their values are quite important for they indirectly influence the number of moves that is accepted and thus the speed of the simulation. As it turns out, the choice which is usually close to optimal is [13],

$$\begin{aligned} \frac{\text{Number of accepted moves}}{\text{Number of attempted moves}} &\cong 0.3 \text{ for particle moves }, \\ \frac{\text{Number of accepted moves}}{\text{Number of attempted moves}} &\cong 0.1 \text{ for volume moves }. \end{aligned} \tag{3.7}$$

One could compute the ratio $\frac{\text{Number of accepted moves}}{\text{Number of attempted moves}}$ after each cycle and change $\delta r_{\max}$ and $\delta V_{\max}$ accordingly to obtain the ratio's given in Equation (3.7). However this procedure would break detailed balance: the probability of going to a certain state after changing these values is not the same as the probability of leaving that state before changing these values. We can thus not measure quantities and change $\delta r_{\max}$ and $\delta V_{\max}$ simultaneously. To solve this problem we use initialization cycles in which the correct values for $\delta r_{\max}$ and $\delta V_{\max}$ are obtained. Note that $\delta r_{\max}$ and $\delta V_{\max}$ are restricted to a maximum value, otherwise the system could grow unbounded. After the initialization cycles are concluded, the actual simulation starts and measurements can be executed.

Whenever we calculate the ensemble average of a quantity in this thesis, we will simulate configurations according to the acceptance rules given by Equations (3.5) and (3.6) (depending on the ensemble we are in). Every step the required quantity is measured and in the end the ensemble average is calculated by the mean value of these measurements.

3.2 Thermodynamic integration

One drawback of Monte Carlo simulations is that they generally do not give you direct access to free energies. For this, MC simulations must be combined with other methods, such as thermodynamic integration. Thermodynamic integration is an approach to find the free-energy difference between two distinctive systems using an auxiliary Hamiltonian and potential.

We consider for example systems A and B with Hamiltonians $\mathcal{H}_A$ and $\mathcal{H}_B$ and potential energies $U_A(\mathbf{r}^N)$ and $U_B(\mathbf{r}^N)$. With these two Hamiltonians we construct a new auxiliary Hamiltonian and auxiliary potential

$$\begin{aligned} \mathcal{H}_\lambda(\Gamma) &= \mathcal{H}_A + \lambda\left(\mathcal{H}_B - \mathcal{H}_A\right), \\ U_\lambda(\Gamma) &= U_A + \lambda\left(U_B - U_A\right) = (1-\lambda)U_A + \lambda U_B. \end{aligned} \tag{3.8}$$

Here Γ indicates a point and phase space and λ is the coupling parameter that allows us to switch from system A to B: at $\lambda = 0$ the auxiliary potential is given by the potential of system

A, while at $\lambda = 1$ potential is given by the potential of system B. Using this order parameter, we can write down the free-energy difference between the two systems A and B:

$$F_{\lambda=1} - F_{\lambda=0} = \int_0^1 d\lambda \frac{\partial F(\lambda)}{\partial \lambda}, \tag{3.9}$$

where $F(\lambda)$ is the Helmholtz free energy of a system with the potential given in Equation (3.8). Making use of the fact that $F = -k_B T \ln Z$, one can show that $F(\lambda)$ is determined by,

$$\exp[-\beta F_\lambda(N,V,T)] = \frac{1}{N!\Lambda^{3N}} \int d\mathbf{r}^N \exp[-\beta \left(U_\mathrm{A} + \lambda \left(U_B - U_A\right)\right)], \tag{3.10}$$

where Λ is the Broglie wavelength. Rearranging Equation (3.10) and taking the derivative of both sides with respect to λ, we find

$$\begin{aligned} \frac{\partial F(\lambda)}{\partial \lambda} &= \frac{\int \mathbf{r}^N \exp\left[-\beta \left(U_\mathrm{A} + \lambda \left(U_B - U_A\right)\right)\right] \left(U_B - U_A\right)}{\int d\mathbf{r}^N \exp\left[-\beta \left(U_\mathrm{A} + \lambda \left(U_B - U_A\right)\right)\right]} \\ &= \left\langle \left(U_B - U_A\right) \right\rangle_\lambda , \end{aligned} \tag{3.11}$$

where $\langle ... \rangle_\lambda$ means that we compute the ensemble average in a system with the Hamiltonian given in Equation (3.8).

To find the free-energy difference between the two systems A and B, we only need to substitute the expression stated in Equation (3.11) into Equation (3.9),

$$F_B(N,V,T) = F_A(N,V,T) + \int_0^1 d\lambda \left\langle \left(U_B - U_A\right) \right\rangle_\lambda . \tag{3.12}$$

In simulations, thermodynamic integration is implemented by performing a numerical integration, using values of the ensemble average $\langle (U_B - U_A) \rangle_\lambda$ determined by MC simulations for a lot of different λ's.

3.3 Wang Landau biasing

When using Monte Carlo simulations, one sometimes wants to obtain information about states that have a really low Boltzmann weight. Because of the fact that configurations are generated according to their Boltzmann weight, the simulation needs to run a long time before the statistics of these rarely visited states become reliable. To solve this problem we can shorten the simulation time by biasing the original potential such that unlikely visited states are visited more often. Afterwards you only have to correct the measured values for the fact that they were obtained in the biased system (something we will come back to later). There are different sorts of bias techniques, but the method we will use here is *Wang Landau biasing* [14]. In the following section we will describe the theory behind this biasing technique.

Obtaining a bias potential

To bias the system we define an 'order' parameter, corresponding to the quantity you want to measure. For example, if you are interested in the average size of a particle, the radius of that particle can be represented by the order parameter. The aim of Wang Landau biasing is to add a biasing potential, η_i, to the potential of every order parameter state i, such that all possible values of the order parameter (or sometimes multiple order parameters), have the same probability. In other words, our aim is to obtain a uniform probability histogram for the system along the order parameter.

When adding a bias potential η_i, the acceptance rule in a Monte Carlo simulation for going from state a to state b changes from Equation (3.4) to

$$acc(a \to b) = \min\left(\frac{f_c(\vec{r_b}^N)}{f_c(\vec{r_a}^N)} \exp\left[-(\eta_a - \eta_b)\right], 1\right). \tag{3.13}$$

To obtain η_i, we use a Monte Carlo simulation: at the start of the simulation η_i is set to zero for all i. At every step an attempt is made to move to another configuration according to the acceptance rule in Equation (3.13). Every n steps the current value of the order parameter is monitored and the bias potential of that state is raised by a certain amount g. Because favorable states are visited more often, the bias potential of these states will be increased more frequently than the biased potential of the unfavorable states and therefore these favorable states become less favorable. By executing this procedure over and over again, in the end one will obtain an approximately uniform distribution.

We now specify the amount g we add to our biasing potential every n steps. To get a sufficiently precise bias potential, it must be possible to have a small value of g: if it would only be possible to add a relatively large value of g, subtle differences could never be obtained. However, if we would start with a small g, the process of flattening the probability distribution would require a lot of time. To solve this problem we allow g to change during the simulation. We start with a relatively large value of g, keeping track of the visits each possible configuration gets. Every n cycles, when we measure the value of the current order parameter and increase the bias potential, we also increase the visits of the state we are in by one (where of course at the beginning of the simulation all visits are set to zero). By doing so you keep track of the time the system spends in a certain state. Whenever the ratio

$$\frac{\text{visits of least visited configuration}}{\text{mean visits of all configurations}} > 0.8,$$

we set $g \to \frac{1}{2}g$ and reset all visits to zero. By doing so we allow the system to both have high and low values of g.

Wang Landau breaks detailed balance condition

If we use Wang Landau as stated above for measuring an ensemble average, there arises a problem. By allowing η and g to change during the simulation, we break detailed balance. The probability of going from state o to state n before changing η is not equal to the probability of going from n to state o after changing η. Just as discussed before while choosing values for $\delta r_{\max}$ and $\delta V_{\max}$, we solve this problem by allowing g and η to change in initialization cycles. When the biased probability histogram is sufficiently flat we fix η and start the real simulation where we measure the desired quantities.

Then of course the question arises what sufficiently flat is and subsequently how long the initialization cycles need to run. Ideally, to obtain a uniform distribution, we want to have g very small (on the order of 10^{-8}), but it turns out that this is computationally very expensive. Fortunately, our goal to begin with was never to obtain a a perfectly flat probability histogram; we only wanted to obtain reliable statistics for unfavorable states. Therefore we just use a large number of initialization cycles and then assume the potential to be flat enough to have all states visited approximately the same number. Of course one has to find out by trial and error what this number of initialization cycles must be, for it depends on the potential you want to bias.

Regaining unbiased results

As already said in the beginning of the section, we need to correct the measured quantities for the fact that the quantities were measured in the biased system. In this thesis, as we will

discuss later, we are interested in the probability ratio between certain states. In the biased system the ratio of probabilities between two states a and b is simply given by

$$\frac{\mathrm{P}_{\mathrm{bias}}(\text{state } a)}{\mathrm{P}_{\mathrm{bias}}(\text{state } b)} = \frac{\text{visits(state } a)}{\text{visits(state } b)},$$

where we measure the visits to each state during the actual simulation. To regain the probabilities in our unbiased system, all we have to do is multiply $\mathrm{P}_{\mathrm{bias}}(\text{state } i)$ by $(\exp[\eta_i])^{-1}$ [14]. Our unbiased ratio is then given by

$$\frac{\mathrm{P}_{\mathrm{unbias}}(\text{state } a)}{\mathrm{P}_{\mathrm{unbias}}(\text{state } b)} = \frac{\mathrm{P}_{\mathrm{bias}}(\text{state } a)\cdot\exp[-\eta_a]}{\mathrm{P}_{\mathrm{bias}}(\text{state } b)\cdot\exp[-\eta_b]} = \frac{\text{visits(state } a)\cdot\exp[-\eta_a]}{\text{visits(state } b)\cdot\exp[-\eta_b]}. \tag{3.14}$$

Initial biasing

Sometimes you already have a clue what form the bias potential will have. Because it can take a lot of time to generate the biasing potential from scratch you can start your Wang Landau biasing with a trial potential η_0 that has roughly the form of the expected potential.

3.4 General characteristics of the simulations

In the next Chapter we will discuss how we implement the techniques considered in this chapter in the actual simulations. However, before we do that, we first need to discuss the general characteristics of these simulation models, such as the treatment of system boundaries.

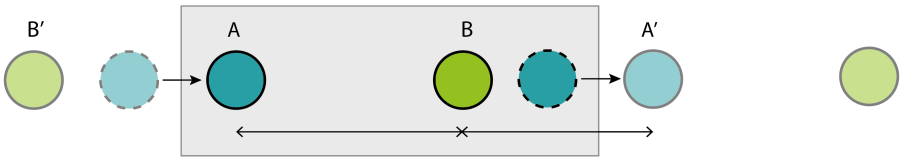

Figure 3.1: *Cartoon of nearest image convention*

Periodic boundary conditions and truncation

As mentioned before, all simulations are implemented with the Monte Carlo algorithm of an NVT-system. The system of such an ensemble consists in this case of a cubic box with sides of length L. We treat the boundaries of the simulation box using periodic boundaries which are implemented via the so called *nearest image convention*. We illustrate this convention by using the example of a one-dimensional box with sides L, displayed in Figure 3.1. In this figure the actual box is indicated as the grey plane. Each particle in the actual system forms interaction pairs with all the other particles. These interaction pairs can either be with particles in the actual system (whenever their inter-particle distance is smaller than half the box length, $L/2$) or with the periodic image of these particles (whenever the inter-particle distance with the actual particle is larger than half the box length). This means that in the specific system displayed in Figure 3.1, particle B forms an interaction pair with particle *A'*, instead of with particle A. Using the same reasoning, particle A then forms an interaction pair with particle *B'*.

Using the nearest image convention implies that particles do not interact with particles at a distance larger than half of the box length. This means that particles do not interact with particles outside the nearest periodic image. When the inter-particle distance is larger than $L/2$, we thus alter the original Yukawa potential and set the interaction energy of that particle pair to zero. However by changing the potential we modify slightly the phase behavior of the system. To solve this problem we need to make our system larger: our original potential goes

to zero for large r, so when $L/2$ is big the change to the potential will be negligible. However, we cannot make the system arbitrarily large for the simulation time depends cubically on the value of L. Therefore we compromise by demanding the potential at $L/2$ is smaller than 10^{-5}. The number of unit cells is chosen such that this requirement is met.

By setting the interaction energy to zero for distances larger than $L/2$, there arises a new problem: At $L/2$ there now opens a gap in the potential, making it discontinuous. To get rid of this discontinuity we lower the potential for distances with $r < L/2$ by the value of the potential evaluated at $r = L/2$. Our potential and force are then given by

$$\frac{\phi(r)}{k_B T} = \Gamma \left(\frac{a}{r}\right) \cdot e^{-\kappa\left(\frac{a}{r}\right)} - U_{\text{cutoff}}$$
$$\frac{\vec{F}(r)}{k_B T} = \left[\left(\frac{a}{r^2} + \frac{\kappa}{r}\right) \cdot \Gamma \cdot e^{-\kappa\left(\frac{r}{a}\right)} - F_{\text{cutoff}}\right] \hat{\mathbf{r}},$$

with,

$$U_{\text{cutoff}} = \Gamma \left[\frac{a}{L/2}\right] \cdot e^{-\kappa\left(\frac{a}{L/2}\right)},$$
$$F_{\text{cutoff}} = \left[\frac{a}{(L/2)^2} + \frac{\kappa}{L/2}\right] \cdot \Gamma \cdot e^{-\kappa\left(\frac{a}{L/2}\right)}.$$

Wigner Seitz constraint

In order to obtain the defect concentration, we need to find the free energy associated with one defect at a specific point in the crystal. This means that to obtain this free energy we need to constrain defects to a specific lattice point, or otherwise the defect could go wander through the crystal. For our simulation this means that we need to constrain particles to the Wigner Seitz cell of their corresponding lattice sites. The Wigner Seitz cell of lattice site m is the area enclosing all points in space that are closer to lattice point m than to all the other lattice points. In the two dimensional crystal of Figure 3.2, for example, the Wigner Seitz area, is given by the green square.

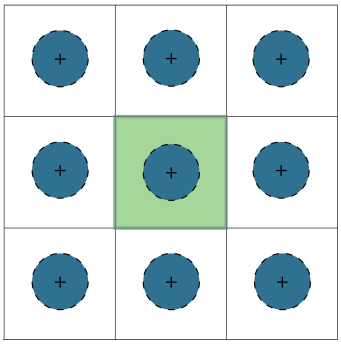

Figure 3.2: *Wigner Seitz cell is indicated by the square green area.*

Using a Wigner Seitz constraint gives rise to a certain concern. In an NVT-ensemble we attempt to move particles every step. However, when one particle at a time is moved, the center of mass will start drifting. Because the Wigner Seitz cells do not move, this means that the centers of the Wigner Seitz cell no longer overlap with the equilibrium positions of the particles. The result is that particles are confined to a volume smaller than the actual Wigner Seitz cell. To stop the drifting of the center of mass we constrain it. In this thesis we do this by moving two particles simultaneously every MC step: one in the direction $+\delta\mathbf{r}$ and the other in the direction $-\delta\mathbf{r}$.

Chapter 4

Calculating the free energies

Now that we have some background on various simulation techniques, we can look at the simulations required to obtain the free energies listed in Section 2.2.2, namely $\mu^{\text{perfect}}(P,T)$, $f^{\text{int}}(\rho_M,T)$ and $f^{\text{vac}}(\rho_M,T)$. In this chapter we discuss for each quantity separately how we will compute it. As it will turn out, the methods of computing $f^{\text{int}}(\rho_M,T)$ and $f^{\text{vac}}(\rho_M,T)$) are almost the same. Therefore we will look in detail at the vacancy case and then just state the results for the interstitial case. In Section 4.1 we will look at how to compute μ^{perfect} and in Sections 4.2 and 4.3 we will discuss respectively how to find $f^{\text{vac}}(\rho_M,T)$ and $f^{\text{int}}(\rho_M,T)$.

4.1 Chemical potential perfect crystal

We find μ^{perfect} via the Gibbs free energy of a perfect crystal. Both quantities are related via the following formula,

$$G^{\text{perfect}} = \mu^{\text{perfect}} N.$$

We cannot obtain G^{perfect} directly, but we can express it in terms of quantities that we can measure, namely F^{perfect} and P:

$$G^{\text{perfect}} = F^{\text{perfect}} + PV.$$

By combining the two equations stated above, we find

$$\mu^{\text{perfect}} = \frac{F^{\text{perfect}} + PV}{N}. \tag{4.1}$$

This means that in order to find μ^{perfect} we need to find both P and F^{perfect} for a perfect crystal. In the following two sections we will discuss how to obtain these quantities.

4.1.1 Helmholtz free energy for a perfect crystal

To find the free energy of a perfect crystal we use, as discussed in Section 3.2, thermodynamic integration. In this case we start with a reference system of which we know the free energy and then integrate from that system to our perfect Yukawa crystal. The reference system we use in this case is the so-called Einstein lattice and therefore we refer to this thermodynamic integration as *Einstein integration* [12]. In this hypothetical Einstein lattice all particles are bound to their lattice sites by a harmonic spring with a certain spring constant α (we will later discuss how to choose the value of α). In the Einstein lattice, the potential energy, called U^{harmonic}, is given by

$$U^{\text{harmonic}} = \sum_{i=1}^{N} \alpha(\mathbf{r}_i - \mathbf{r}_{i,0})^2,$$

where $\mathbf{r}_{i,0}$ is the lattice position of particle i and $\mathbf{r}_i$ is the particle position of particle i. We rewrite the auxiliary potential, given in Equation (3.8), for this specific system,

$$U^{\text{int}}(\mathbf{r}^N) = (1-\lambda)U(\mathbf{r}^N) + \lambda U^{\text{harmonic}}(\mathbf{r}^N), \tag{4.2}$$

where $U(\mathbf{r}^N)$ is the the potential energy of the Yukawa system given by Equation (2.2). Again λ is the switching parameter that switches between the Yukawa crystal, when $\lambda = 0$, and the Einstein lattice, when $\lambda = 1$.

Using Equation (3.12) we find

$$F_{\text{Yukawa}} = F_{\text{Einstein}} - \int_0^1 d\lambda \left\langle U^{\text{harmonic}}(\mathbf{r}^N) - U(\mathbf{r}^N) \right\rangle_\lambda . \tag{4.3}$$

Fixed center-of-mass frame

When we use Equation (4.3), there arises a certain problem. Whenever λ is close to zero, the springs do not constrain the particles to their lattice sites any longer, potentially causing the center of mass to start drifting. Note that this is possible because in this case particles are not bound to stay in a Wigner Seitz cell. The drifting of the center of mass causes $\langle r^2 \rangle$, and thus the potential energy difference $\left\langle U^{\text{harmonic}}(\mathbf{r}^N) - U(\mathbf{r}^N) \right\rangle_{\lambda \to 0}$, to be potentially very big compared to the rest of the computed energy differences. Due to this sharp energy peak, the integral in Equation (4.3) becomes hard to evaluate. One way of solving this problem is by requiring small integration steps for $\lambda \to 0$. In this case, however, we adopt another method and solve the problem by going to the center of mass frame. Note that it would also be possible to fix the center of mass, however here we elect to go to the center of mass frame. By doing so we bound the value of $\langle r^2 \rangle$ and thus reduce the peak of the integrand. Fixing the center of mass changes Equation (4.3) to

$$F^{\text{CM}}_{\text{Yukawa}} = F^{\text{CM}}_{\text{Einstein}} - \int_0^1 d\lambda \left\langle U^{\text{harmonic}}(\mathbf{r}^N) - U(\mathbf{r}^N) \right\rangle^{\text{CM}}_\lambda , \tag{4.4}$$

where $F^{\text{CM}}_{\text{Yukawa}}$ is the Helmholtz free energy of a Yukawa crystal obtained in a fixed center of mass frame, F_{Einstein} is the Helmholtz free energy of an Einstein crystal obtained in a fixed center of mass frame. Here $\langle ... \rangle^{CM}_\lambda$ indicates that the ensemble average is calculated in the center of mass frame and evaluated using the potential given in Equation (4.2).

The value of $F^{\text{CM}}_{\text{Yukawa}}$ however differs from F_{Yukawa} and we are interested in the latter. To regain F_{Yukawa} out of $F^{\text{CM}}_{\text{Yukawa}}$ is quite a long calculation and it does not provide much insight for this thesis. We therefore omit the derivation and only state the results. In Ref. [15] it is obtained, using the expression of Equation (4.4), that for a three dimensional single component system of identical particles and spring constant α, F_{Yukawa} is given by

$$\begin{aligned} \beta F_{\text{Yukawa}} = \frac{3N}{2} \ln\left(\frac{\alpha\beta\Lambda^2}{2\pi}\right) - \beta \int_0^1 d\lambda \left\langle U^{\text{harmonic}}(\mathbf{r}^N) - U(\mathbf{r}^N) \right\rangle^{CM}_\lambda - \\ \frac{3}{2} \ln\left(\frac{\alpha\beta}{2\pi}\right) - \frac{3}{2} \ln N + \ln N/V, \end{aligned} \tag{4.5}$$

with Λ is the de Broglie wavelength. In this formula, the first term corresponds to $F^{\text{CM}}_{\text{Einstein}}$ and the last three terms are corrections due to the fact that we are in the center-of-mass system.

Choosing parameters

Finally we need to specify how to choose the value for α. This value does not matter too much, and there are only two requirements. First, the crystal may not melt for any value of λ, which means α must be sufficiently high - something that can be tested by looking at

snapshots of the particles during the simulation to check that the system stays a crystal. The second requirement is that for $\lambda \to 1$ the system must behave like an Einstein crystal. This can be checked by computing the free energy of the Einstein crystal for λ's close to 1 during the simulation and comparing those with the theoretical values of an Einstein crystal.

To numerically evaluate the integral in Equation (4.5), we first make a change of variables to flatten the integrand and then use a certain method called *the Gaussian quadrature*. What this method basically does is choosing suitable points to evaluate the integral. We will not elaborate any further on this method nor the change of variables, but the entire procedure is explained very well in Chapter 10 of Ref. [12]. The only thing important for this thesis is that by making the change of variables there occurs an extra parameter c that we choose such that the integral is as flat as possible. There exists a tested code, written by Frank Smallenburg, that makes the change in variables and then evaluates the integral using the Gaussian quadrature method. In this thesis we will use this program to obtain the required values for βF_{Yukawa}.

4.1.2 Pressure of a perfect crystal

To find the pressure of a perfect crystal we use the virial expression for the pressure [16],

$$\frac{P}{k_B T} = \rho + \frac{\beta}{3V}\overline{\sum_{i<j} \mathbf{f}_{ij} \cdot \mathbf{r}_{ij}}, \tag{4.6}$$

with ρ the density and $\mathbf{f}_{ij}$ and $\mathbf{r}_{ij}$ respectively the force, given by Equation (2.3), and the distance between particles i and j. To obtain the $\beta/(3V)\overline{\sum_{i<j} \mathbf{f}_{ij} \cdot \mathbf{r}_{ij}}$ term, we perform a Monte Carlo simulation measuring the ensemble average of $\langle \sum_{i<j} \mathbf{f}_{ij} \cdot \mathbf{r}_{ij} \rangle$ for a Yukawa crystal. Because the simulation is performed in an NVT-ensemble, ρ is then determined by the defined values of N and V.

Simulating the expressions of Equations (4.5) and (4.6) and then combining them via Equation (4.1) for various values of κ and Γ, provides us with the required values for μ^{perfect}.

4.2 Calculating f^{vac} - Free energy associated with one vacancy

In this section we will discuss the simulations we need to perform in order to obtain the free energy $f^{\text{vac}}(\rho_M, T)$. This free energy, is given by the difference between the Helmholtz free energy of a perfect crystal and a crystal with one vacancy at a specific lattice site,

$$f^{\text{vac}}(\rho_M, T)) \equiv F^{\text{vacancy}} - F^{\text{perfect}}.$$

To calculate this energy difference, we use two steps. First we calculate the energy difference, f^{shrink}, associated with the free energy between a crystal with one non-interacting particle (i.e. an ideal gas particle with $\Gamma = 0$) and a perfect crystal and then we calculate the energy, f^{remove}, associated with removing this ideal particle from the crystal. In order words,

$$f^{\text{vac}}(\rho_M, T)) = f^{\text{shrink}} + f^{\text{remove}}. \tag{4.7}$$

The process described above is schematically displayed in Figure 4.1. In Section 4.2.1 we will discuss how to obtain f^{shrink} and in Section 4.2.2 we will discuss how to compute f^{remove}.

4.2.1 Free energy of turning a particle into an ideal gas particle

In this section we will discuss how to compute the free energy f^{shrink}. Because there is no data available to check our obtained values with, we will to compute f^{shrink} using two different, independent ways. By checking if these two methods agree with one another, we can check if

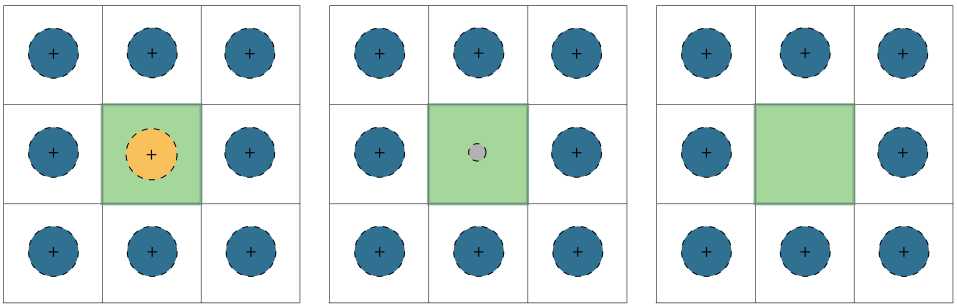

Figure 4.1: *Schematic process of calculating $f^{vac}(\rho_M, T)$. In the left figure we start with a perfect crystal. The particle with no interactions is then represented as the grey particle in the middle figure. Finally in the right figure, the non-interacting particle is removed from the system. f^{shrink} is the free energy difference between the first two figures and f^{remove} is the free energy difference between the last two figures.*

no mistakes were made during the coding and simultaneously we can see which method works best for the actual simulations. In the next chapter, Chapter 5, this choice of method will be discussed. The two methods that we use, are thermodynamic integration and calculating the ratio of probabilities between having a normal particle and a non-interacting particle. Both methods will be discussed in the two following sections.

Method 1 - Thermodynamic integration

For the thermodynamic integration we again use the theory described in Section 3.2. In this specific case Equation (3.8) is given by

$$U_\lambda(\Gamma) = (1-\lambda)U_{\text{perfect}} + \lambda U_{\text{vacancy}}, \tag{4.8}$$

with U_{perfect} the potential energy of a perfect crystal, and U_{vacancy} the potential energy of a crystal with one vacancy[1]. According to Equation (3.12), the free-energy difference between a crystal with one non-interacting particle and a perfect crystal is then given by,

$$f^{\text{shrink}} = F^{\text{non-interacting}} - F^{\text{perfect}} = \int_0^1 d\lambda \left\langle (U_{\text{vacancy}} - U_{\text{perfect}}) \right\rangle_\lambda , \tag{4.9}$$

with $F^{\text{non-interacting}}$ the Helmholtz free energy of a crystal containing one non-interacting particle. The ensemble average, $\langle ... \rangle_\lambda$ is evaluated using the auxiliary potential given in Equation (4.8).

Although in theory this method works fine, in practice there arises a problem that requires the simulation to run for a long time. When the system is at $\lambda = 0$ we are evaluating ΔU using the potential $U_{\lambda=0} = U_{\text{vacancy}}$. This means that without any energy penalty, the non-interacting particle can come very close to other particles if those particles are near their Wigner Seitz cell boundary. Because we compute the potential energy difference with the system where our particle does have interactions, the term $\langle (U_{\text{vacancy}} - U_{\text{perfect}}) \rangle_{\lambda=0}$ can become very large - in the interstitial case even infinitely large. Duo to these (infinitely) large energy differences, the simulation needs a long, or potentially even infinitely long, time to get a reliable answer for the value $\langle (U_{\text{vacancy}} - U_{\text{perfect}}) \rangle_{\lambda=0}$.

[1] Because the non-interacting particle contributes nothing to the potential energy, we can just use the potential energy of a crystal with a vacancy instead of the potential energy of a crystal with one non-interacting particle.

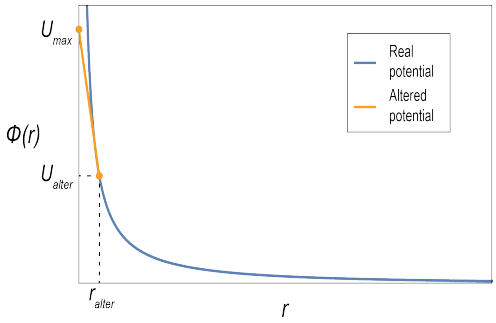

Figure 4.2: *Cartoon of defects in a crystal*

To solve this problem we alter the potential. Instead of letting it to diverge at $r = 0$ as it normally would do, we assume that the potential increases linearly below a certain defined value r_{alter}. By doing so the potential has a finite value, U_{max}, at $r = 0$. The altered potential is displayed in Figure 4.2 where we have defined U_{alter} as $U(r_{\text{alter}})$. If we evaluate $\langle (U_{\text{vacancy}} - U_{\text{perfect}}) \rangle_{\lambda=0}$ for higher λ's this altered potential will not have any influence for the particles will never have a distance r with $r < r_{\text{alter}}$ due to the energy penalty. However for small λ, we avoid the (infinitely) large energies. Because in the end we integrate over the energy difference (see Equation (4.9)), this alteration to the potential will have no influence. The precise values for U_{max} and r_{alter} do not matter that much, as long as we make sure r_{alter} is so small that for higher values of λ, r will almost never be smaller than r_{alter}. We can check this by running the same simulation twice for slightly different values of U_{max} and r_{alter}. If the values are chosen alright, they should give the same answer up to a reasonable accuracy.

Method 2 - Ratio of probabilities

For the second method for calculating f^{vac}, we use the fact that the Helmholtz free energy of a state is proportional to the logarithm of the partition function of that state. This means that the free-energy difference between two states, A and B, is given by the logarithm of the ratio of the corresponding partition functions, Z, and thus the ratio of the corresponding probabilities of those states [2]. This means that,

$$\Delta F^{AB} \equiv F^A - F^B = k_B T \log \frac{Z^B}{Z^A} = k_B T \log \frac{P^B}{P^A}, \tag{4.10}$$

where P^i is the probability of being in state i. We can thus obtain the value f^{shrink}, by finding the ratio of probabilities between $P^A = P(\Gamma_{\text{var}} = 0)$ and $P^B = P(\Gamma_{\text{var}} = \Gamma)$, with Γ_{var} the dimensionless interaction energy of our shrinking particle.

We name the particle that turns into a non-interaction particle γ. One might think that we can just compute the probability ratio by performing a Monte Carlo simulation where we allow the interaction energy of γ to be in either a state with $\Gamma_\gamma = 0$ or a state with $\Gamma_\gamma = \Gamma$. However unfortunately this is not the case for the energy the state where $\Gamma_\gamma = 0$ is much lower than the state where $\Gamma_\gamma = \Gamma$. When we simulate this system, we would always end up in the non-interacting state, meaning that the obtained statistics would be unreliable. In order to get the correct probability thus alter our simulation:

1. First we allow the particle γ to have a range of different interaction energies between 0 and Γ. Every n Monte Carlo cycles we try to increase or decrease the current Γ_i to either Γ_{i+1} or Γ_{i-1}. By doing so, the energy barrier of switching to another Γ_i is smaller, which makes the move more likely to happen compared to the case when it only could switch between 0 and Γ. The precise number of possible Γ_i's does not matter much as long as it is not too small for then the energy barrier between different Γ_i's is still too high.[3] The precise value of n does not matter either, as long as it is big enough for the system to change in between switching attempts of Γ_i.

2. Secondly we apply the Wang Landau biasing discussed in Section 3.3. In this case the order parameter is defined as the interaction energy of particle γ. We want to bias the

[2] The probability P^i of being in state i is equal to $Z^i / \sum_i Z^i$ with $\sum_i$ the sum over all possible states.

[3] Note however that one cannot choose an arbitrarily large number of possible Γ_i's, because then the problem arises that it will take too much time to visit all different Γ_i's.

potential such that the probability histogram of Γ_i is approximately flat. In the biased system we then measure the ratio of probabilities.

By performing the Monte Carlo simulation with the two alterations mentioned above we can obtain $k_B T \log \frac{P(\Gamma=\Gamma)}{p(\Gamma_{\text{var}}=0)}$, providing us a with a second measurement of f^{shrink}.

4.2.2 Energy of removing ideal gas particle

The second step in computing $f^{\text{vac}}(\rho_M, T)$ is obtaining a value for the free energy, f^{remove}, associated with removing an ideal gas particle from the crystal. It can be shown that the free energy of an ideal gas particle constrained to a Wigner Seitz cell is given by

$$f^{\text{ideal gas}} = -k_B T \ln\left(\frac{V^{WS}}{\Lambda^3}\right),$$

with V^{WS} the volume of the Wigner Seitz cell. Removing such a particle from the system, means that you lower the free energy of that system by an amount $f^{\text{ideal gas}}$. Therefore we can see that,

$$f^{\text{remove}} = -f^{\text{ideal gas}} = -\left[-k_B T \ln\left(\frac{V^{WS}}{\Lambda^3}\right)\right]. \tag{4.11}$$

Because we are in an NVT-ensemble, the volume of a Wigner Seitz cell, defined by V/N, is just a constant. This means that we can obtain f^{remove} without having to perform any simulations.

With the expression in Equation (4.11) have now all the information we need to calculate $f^{\text{vac}}(\rho_M, T)$. In the last section of this chapter we turn our attention to the computation of the energy associated with an interstitial.

4.3 Calculating f^{int} - Free energy associated with one interstitial

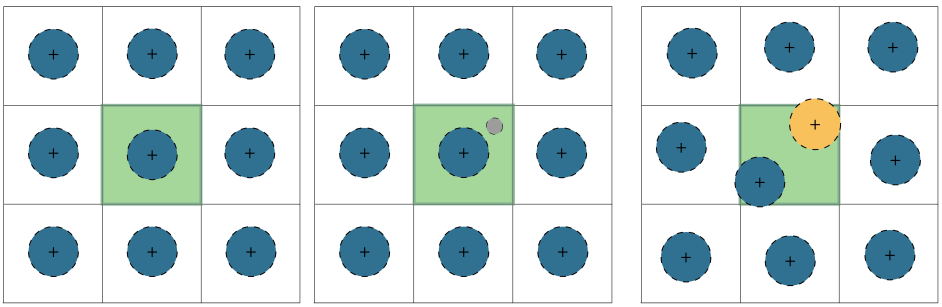

Figure 4.3: *Schematic process of calculating $f^{int}(\rho_M, T)$). In the left figure we start with a perfect crystal. In the middle figure a particle with no interactions, represented as the grey particle, is inserted in the system. Finally in the right figure, the non-interacting particle has turned into a normal particle. f^{insert} is the free-energy difference between the first two figures and f^{grow} is the free-energy difference between the last two figures.*

The method of calculating the free energy associated with one interstitial, f^{int}, is, as already said, almost the same as the method of calculating f^{vac}. In this case we insert a non-interacting particle into a specific Wigner Seitz cell of a crystal and then let the interaction energy of that particle grow from 0 to Γ. This procedure is schematically displayed in Figure 4.3. Comparing the process in the case of an interstitial with that of a vacancy, we see that there are only two differences.

1. The process of calculating f^{int} is reversed compared to computing f^{vac} . In this case we insert a non-interacting particle into a Wigner Seitz cell and then let the interaction energy of that particle increase.

2. The cell where we insert and grow the particle is not empty as it was in the vacancy case, but already contains a normal interacting particle. This means that we need to include this extra particle in our simulations.

The energy associated with an interstitial, f^{int}, is now given by $f^{\text{insert}} + f^{\text{grow}}$, where f^{insert} is the free energy associated with inserting a non-interacting particle to our system and f^{grow} is the free-energy difference between a crystal with an interstitial and a crystal with a non-interacting interstitial. In the following two sections we will briefly discuss how to obtain f^{insert} and f^{grow} using the same methods as we did in the vacancy case.

Method 1 - Growing a particle

We again use the fact that the logarithm of the ratio of probabilities is connected to a free-energy difference. In this case f^{grow} is thus given the ratio of probabilities between having a normal interstitial and an interstitial with no interactions:

$$f^{\text{grow}} = F^{\text{interstitial}} - F^{\text{non-interacting interstitial}} = k_B T \log \frac{P(\Gamma_{\text{var}} = 0)}{P(\Gamma_{\text{var}} = \Gamma)},$$

with Γ_{var} the interaction energy of the inserted particle. The procedure of finding this ratio of probabilities is the same as in the vacancy case.

Method 2 - Thermodynamic integration

For the method of thermodynamic integration we again we use Equation (3.12), with in this case $U_\lambda = (1-\lambda)U_{\text{perfect}} + \lambda U_{\text{interstitial}}$. This means that

$$f^{\text{grow}} = \int_0^1 d\lambda \left\langle (U_{\text{interstitial}} - U_{\text{perfect}}) \right\rangle_\lambda ,$$

where we can use U_{perfect} as the potential energy of the crystal with the non-interacting particle, for the non-interacting particle again contributes nothing to the potential. In this case again we use the altered potential given in Figure 4.2 instead of our normal potential to avoid infinitely large energies.

Free energy associated with inserting a non-interacting particle

The free energy associated with inserting a non-interacting particle is minus the energy associated with removing that particle. Using Equation (4.11), we see that this means that

$$f^{\text{insert}} = -k_B T \ln \left(\frac{V^{WS}}{\Lambda^3} \right). \tag{4.12}$$

This concludes our discussion of the various methods required for measuring $\mu^{\text{perfect}}(P,T)$, $f^{\text{int}}(\rho_M, T)$ and $f^{\text{vac}}(\rho_M, T)$. In the next chapter we will first discuss some checks we did to verify the various simulations and then later turn our attention to the results.

Chapter 5

Results & Discussion

As stated earlier, we begin this chapter with the discussion of various checks that we used to validate the simulations. We verify these simulations for two reasons: first of all we check that no mistakes were made during the coding and secondly we check if the applied methods work in these specific cases. Although from a theoretical point of view all the methods described in the previous chapter should work correctly, it turns out that in practice, due to the characteristics of the specific system, not all simulations perform equally well. A program can, for example, be computationally very expensive in a specific system, making the corresponding method not suitable for that system. In Sections 5.1.1 and 5.1.2 we first briefly discuss some very basic checks concerning respectively the simulation of an NVT-ensemble and Wang Landau biasing and in Section 5.1.3 we then test the validity of the Einstein integration program.
After these checks we turn our attention in Section 5.2 to the discussion of which of the two possible methods to compute f^{shrink} and f^{grow} we will use. Finally, we end this chapter with Section 5.3 where we list and discuss the computed defect concentrations and look at how the defects manifest themselves in the crystals.

5.1 Validity checks

5.1.1 *NVT*-ensemble of Yukawa crystal

As said before, the basis of all our simulations is a crystal in an NVT ensemble with particles interacting via a Yukawa potential. In order to find f^{shrink} and f^{grow}, we therefore need to make sure that we have this system working correctly. First we check if the simulation of an NVT ensemble works correctly by simulating an NPT-ensemble (which has an NVT-ensemble included) for hard spheres. In this simulation we calculate the equation of state and compare the results with the theoretical approximation of the equation of state. This procedure is shown in Appendix A. Thereafter we include the Yukawa potential of soft particles in the simulation and compare the energy of this system with the data from the paper of Hamaguchi, Fraouki and Dubin (1997) [10]. This comparison can be found in Appendix B. The conclusion of both checks is that the simulation of a crystal with Yukawa particles living in an NVT-ensemble is correct.

5.1.2 Wang-Landau biasing

Because the coding of the simulation to obtain the Wang Landau biasing is quite complicated, we first check the simulation separately for a system where we already know what the original potential looks like. We can then check whether the real potential and the bias potential together form a uniform distribution and thus whether our simulation works correctly. This test is shown in Appendix C and again the conclusion is that our simulation is working correctly.

5.1.3 Validating Einstein integration

To ensure that the Helmholtz free energy of the Yukawa crystal, obtained via Einstein integration, is computed correctly, we check the simulation by comparing the results with the virial pressure of the system. Besides the validation of the Helmholtz free energy, this check thus also provides us with a check of the pressure computation. We know from thermodynamics that in an NVT ensemble,

$$\beta\frac{\partial F}{\partial V} = -\beta P \text{ and } dV = -\frac{N}{\rho^2}d\rho.$$

This means that the difference in free energy between two systems with different densities, ρ_1 and ρ_2, is given by,

$$\beta\frac{F(\rho_2) - F(\rho_1)}{N} = -\beta\int_{\rho_1}^{\rho_2} d\rho' \frac{P(\rho')}{\rho'^2}. \tag{5.1}$$

For this test we obtain the free energies in the left hand site of Equation (5.1) by calculating the Helmholtz free energy for two different densities (ρ_1 and ρ_2) via Einstein integration. To obtain the integral of the right hand side of the equation, we compute the pressure for a number different densities between ρ_1 and ρ_2 and perform a numerical integral using that data. The pressure is computed using the virial expression given in Equation (4.6). Note that because we look at how density influences the system, it is convenient to use the Yukawa potential given in Equation (2.1) with the 'normal' parameters instead of the dimensionless parameters. By checking if the simulated values of the left and the right hand side of Equation (5.1) agree with each other we can validate that the Einstein integration works correctly.

We calculate F for two different values of ρ, namely $\rho_1 = 0.239$ (corresponding to a Wigner Seitz radius of 1) and $\rho_2 = 0.179$ (corresponding to a Wigner Seitz radius of 1.1). The point in the phase diagram we look at is determined by $\kappa_D = 4$ and $\epsilon = 13000$, which means that for both densities we are looking at an FCC-crystal. We obtain, using Einstein integration:

$$\beta\frac{F(\rho_2) - F(\rho_1)}{N} = 19.062 \tag{5.2}$$

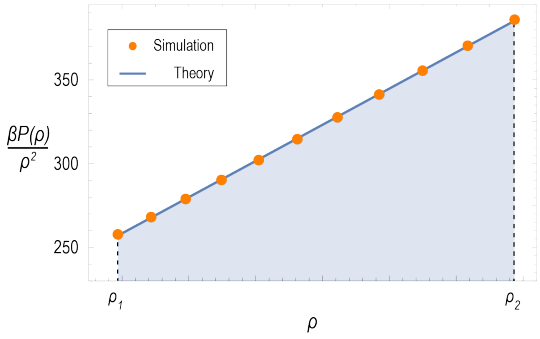

Figure 5.1: *Integral over* $\frac{P(\rho')}{\rho'^2}$ *from* ρ_1 *to* ρ_2

The data provided by the pressure calculation is displayed in Figure 5.1. In this figure, the value of the integral of the right hand side of equation (5.1.3) is schematically represented as the blue surface area and is equal to[1]

$$-\beta\int_{\rho_1}^{\rho_2} d\rho' \frac{P(\rho')}{\rho'^2} = 19.070 \tag{5.3}$$

Comparing the numerical values of Equations (5.2) and (5.3), we see that the difference between the two methods is 0.008. During the Einstein simulations we saw that the chosen constants (α and c) influence slightly the outcome of the Einstein integration on the order of 0.01. This most probably explains the difference between Equations (5.2) and (5.3). For the calculations of the defect concentration we do not need precision up to second order decimals, and therefore we can conclude that our Einstein integration and the pressure calculation agree with each other up to the desired accuracy and thus that both simulations work correctly.

[1] We have calculated P with and without particles constrained to their Wigner Seitz cell. It turns out that this constrain has no influence on the pressure

5.2 Wang Landau Biasing versus thermodynamic integration

We now turn our attention to which of the two methods discussed in Section 4.2.1 we are going to use to calculate f^{shrink} and f^{grow}. In order to compare the two methods, we calculate f^{shrink} with both methods for a specific point in a BCC Yukawa crystal determined by $\kappa = 3.0$ and $\Gamma = 1300$. In Figure 5.2 we display the data obtained with both methods. For the method of thermodynamic integration, we plot in Figure 5.2a, $\beta\langle\Delta U\rangle = \beta\left\langle\left(U_{\text{vacancy}} - U_{\text{perfect}}\right)\right\rangle_\lambda$ as a function of λ, with λ the earlier defined switching parameter. In Figure 5.2b the bias potential, $\beta\eta(\Gamma)$, obtained via Wang Landau biasing is plotted as a function of Γ.

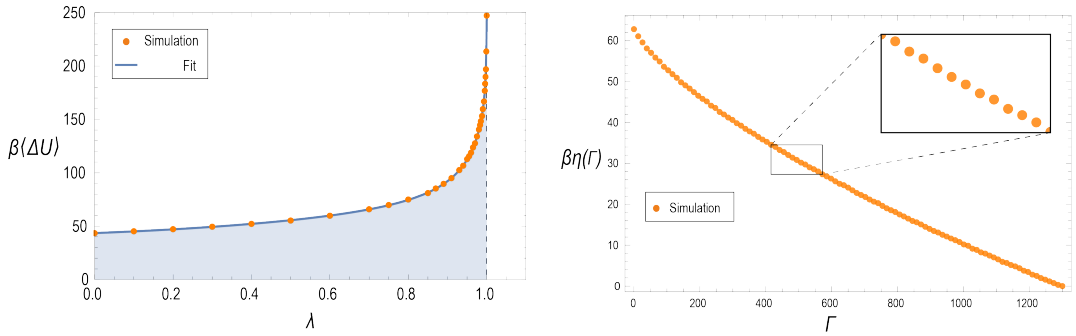

(a) *Thermodynamic integration*

(b) *Wang Landau biasing*

Figure 5.2: *Two methods for calculating* f^{shrink}

Results

To obtain f^{shrink} with the method that uses Wang Landau biasing, we use the values of the bias potential and the number of visits, displayed in Figure 5.4, both at $\Gamma = 0$ and $\Gamma = 1300$. With them we evaluate Equations (4.10) and (3.14). To find f^{shrink} using thermodynamic integration, we need to evaluate the integral stated in Equation (4.9), graphically represented by the area of the blue plane in Figure 5.2a. We obtain the following results with both methods

$$\beta f^{\text{shrink}}_{\text{Wang Landau}} = -62.51,$$
$$\beta f^{\text{shrink}}_{\text{thermodynamic}} = -63.67.$$

As we can see they differ by around 1, which means that they do not agree as well as we had hoped. Although in principle this could mean that both methods work incorrectly, we are almost positive we can explain this difference by the fact that the Wang Landau method proves to be very slow in this system.
When we bias the system using Wang Landau biasing we want all different values of the interaction energy of the shrinking particle to have approximately the same probability. Whenever a particle is constrained to a small volume (due to a large value of Γ) it is not that hard to bias the state: the potential that a

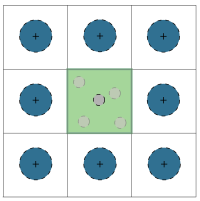

Figure 5.3: *Cartoon of particle position for* $\Gamma = 0$

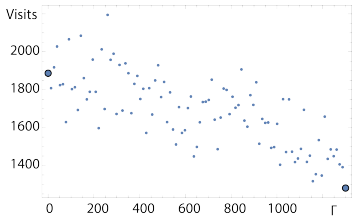

Figure 5.4: *Visits to a certain configuration as a function of* Γ. *The big dots indicate the visits of respectively* $\Gamma = 0$ *and* $\Gamma = 1300$

particle feels does not change that much when the particle moves around in a small volume. However in the case when $\Gamma = 0$, the shrinking particle can move through the entire Wigner Seitz volume (see Figure 5.3). The potential that the particle feels depends enormously on the position of the particle. This means that we can never find an perfect biasing potential. Ideally in this case you would calculate a separate biasing potential for every possible position of the shrinking particle (which means that you get an extra order parameter in your system), however this is not feasible. The other option is to let your program run longer to improve your statistics.

We tried to improve the statistics by letting the simulation run for a week, but even that turned out to be too short to obtain enough data: the value of $\beta f^{\text{shrink}}_{\text{Wang Landau}}$ that we obtained after half a week of running was equal to $\beta f^{\text{shrink}}_{\text{Wang Landau}} = -62.71$. This results differs 0.2 from the value obtained after a week of running, implying that the system, even after a week of running, had not obtained enough statistics. This conclusion is supported by the data in Figure 5.4, where we look at the visits as a function of Γ obtained after a week of running. Although a trend is clearly visible, the error of the visits is very big, indicating that we do not have enough statistics. Concluding, it is most likely that the difference between the two methods is due to the fact that Wang Landau biasing is not a good method for this specific system. For some systems it is a very useful method, however when, for a constant order parameter, the energy of the system fluctuates too much (as it does in this case) the simulation needs too long of a time to run.

In contrast to the Wang Landau biasing method, the thermodynamic integration simulation did have enough statistics after about 24 hours of running. It seems thus to be obvious that thermodynamic integration is the best choice to compute f^{grow} and f^{shrink}. However, before we continue with this method, we need to check separately that no mistakes were made during the coding. Because we can no longer compare it with the Wang Landau method we need to check it with other independent checks. Berend van der Meer wrote a simulation that also uses thermodynamic integration to compute f^{shrink} and his result did agree with our result. Thereafter Laura Filion used a separate method, namely Einstein integration, to compute the energy associated with one interstitial[2], f^{int}. We compared her result with the value for f^{int} we found using thermodynamic integration and found that both values agree reasonably. We may thus conclude that the code for thermodynamic integration works correctly and therefore we will proceed with this method to calculate the concentration of defects.

5.3 Outcomes

Now that we may conclude that our simulations work correctly, we can turn our attention to the actual questions we want to address. From Chapter 4 it became clear that to find the defect concentrations we need to perform three different simulations: Einstein integration to obtain F^{Perfect}, thermodynamic integration to obtain f^{vac} and f^{int} and finally a simple Monte Carlo simulation to obtain the pressure. Before we go to the results we first briefly discuss the initial conditions used for each of these simulations. In Section 5.3.1 we will then list and discuss the obtained defect concentrations and finally we end the chapter with Section 5.3.2 where we look at how the crystalline ordering of particles changes due to the presence of point defects.

As said in the introduction, we are interested in the concentration of vacancies and interstitials around both the fluid-BCC and BCC-FCC/fluid-FCC phase boundaries, as we expect that the concentration will be the highest there. We obtain the phase points along the phase boundary, using the coexistence lines stated in Ref. [11]. These curves, although fitted on the coexistence points obtained in Ref. [10], do slightly differ from these points. It might seem wrong to use the fitted curves because of this deviation. However it turns out that the

[2]Note that in the case of Einstein integration we do not use a perfect crystal as one of the endpoint of thermodynamic integration, but a crystal with with an interstitial.

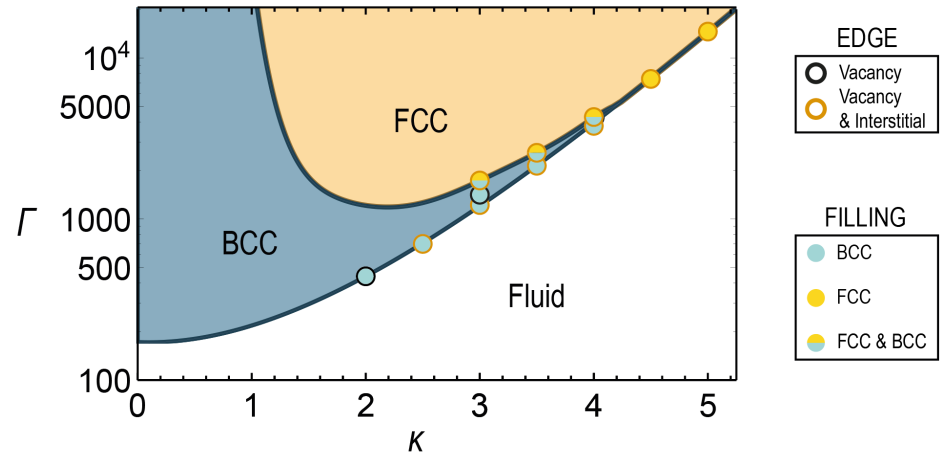

Figure 5.5: *Points where defect concentration is computed*

actual model has a coexistence *region* rather than a coexistence *line*[3] and therefore being a little above or below the coexistence line or points presented in the papers does not make the crystals immediately unstable. As long as we check that the simulated crystal is (meta) stable by looking at snapshots of the simulation, it is therefore possible to use the points as well as the curves as the phase points for our actual simulation. In this case we have chosen to simply use the curve to obtain points along the phase boundary.

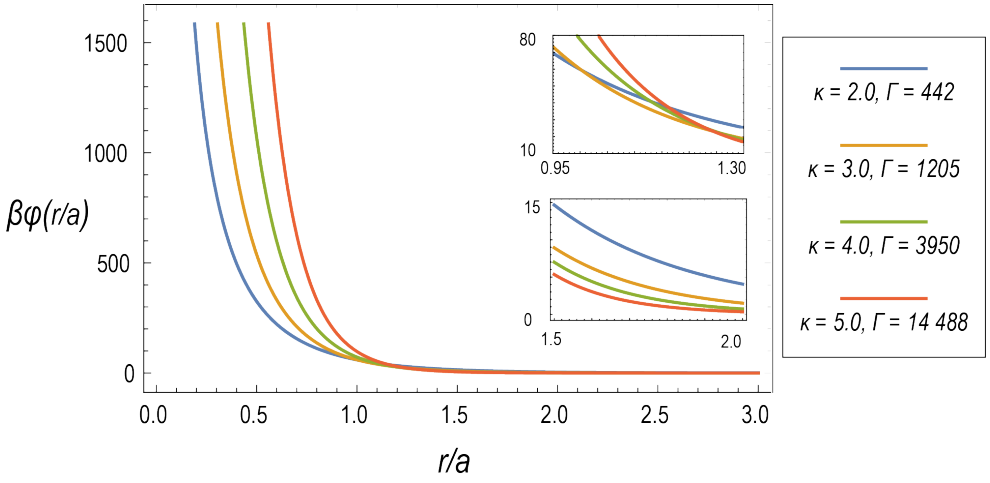

Figure 5.6: *Yukawa potential plotted for different values of* κ *and* Γ.

All the points for which we evaluated the concentration of vacancies, interstitials or both are displayed in Figure 5.5. As one can see, we only look at respectively high values of κ ($\kappa \geq 2$). Going to lower κ, exponentially increases the interaction range and thus the system size and simulation time. Due to lack of time we therefore could not go to the (very) low κ regimes. To give some impression of how the potential looks like for different (κ, Γ)-points we plot the potential in Figure 5.6 for some of the evaluated points.[4] As we can see, going to higher (κ, Γ)-points makes the potential steeper.

[3]The coexistence region is quite narrow compared to the the rest of the phase diagram and therefore we display it as a line in the diagram.

[4]Note that these are unaltered potentials; no cutoff or truncation is used.

Table 5.1: *Cutoff values of simulations*

κ	Γ	Cutoff BCC	Cutoff FCC
2.0	442	$8.12/a$	-
2.5	708	$7.11/a$	-
3.0	1205	$6.09/a$	-
	1720	$6.09/a$	$6.40/a$
3.5	2143	$5.08/a$	-
	2565	$5.08/a$	$6.40/a$
4.0	3950	$5.08/a$	-
	4234	$5.08/a$	$6.40/a$
4.5	7438	-	$6.40/a$
5.0	14488	-	$6.40/a$

Initial conditions

We now give a general overview of the initial condition for each of the simulations (thermodynamic integrations, Einstein integration and the pressure simulation). For the thermodynamic integration and the pressure simulation the following initial conditions were used[5]:

- *System size*: As stated earlier, the system size was chosen such that the error due to the cutoff of the potential was smaller than 10^{-5}. In practice this meant that, depending on the phase point and the crystal type, the simulations contained between 250 and 1024 particles. The values of the cutoff length in units of a are listed in Table 5.1 for all evaluated points.

- *Initialization cycles*[6]: The number of initialization cycles used to obtain $\delta r_{\max}$ and $\delta V_{\max}$ did lie around 10.000.

- *Cycles*: The simulation ran for between $3 \cdot 10^5$ cycles (for a vacancy simulation with λ close to zero) and $2 \cdot 10^6$ cycles (for an interstitial simulation with λ close to one). For each phase point it was checked that the system was well equilibrated.

- $U_{\max}$ and U_{alter}: For vacancies we used $U_{\max} = 3{\cdot}10^4$ and $U_{\text{alter}} = 9{\cdot}10^3$. For interstitials we used $5 \cdot 10^4 \leq U_{\max} \leq 8 \cdot 10^4$ and $3 \cdot 10^4 \leq U_{\text{alter}} \leq 5 \cdot 10^4$. Here the lower regime of $U_{\max}$ and U_{alter} was used for low values of κ and Γ and the higher regime was used for high values of κ and Γ. We checked that for higher values of $U_{\max}$ and U_{alter}, the concentration of vacancies or interstitials did not change significantly.

- *Integration steps*: We evaluated the thermodynamic integral using 34 points. In the regime where the shrinking/growing particle behaved like it was non-interacting we used $\Delta\lambda = 0.01$, whereas in regime where it had interactions we used $\Delta\lambda = 0.1$.

For the Einstein integration simulation the following initial conditions were used.

- *System size*: The system size for each phase point in the Einstein integration simulation was chosen such that it matched the system size in the corresponding thermodynamic integration simulation.

- *Cycles*: The number of cycles used for each point was 10^5.

- As stated earlier the constants α and c were chosen such that the system did not melt and the integrand was sufficiently flat. In this case we used $\alpha = 2000$ and $c = 1$.

[5]Note that for a lot of these initial conditions the precise value does not matter much as long as you check that the system is well equilibrated.

[6]In this case one cycle corresponds to N Monte Carlo steps with N the number of particles.

- *Gaussian points*: We have not discussed the Gaussian quadrature method in this thesis, but for the interested reader, the number of points used to evaluate the integral was equal to 20.

5.3.1 Defect concentrations

The values obtained for the defect concentrations together with the values for $\mu^{\text{perfect}}(P,T)$, $f^{\text{vac}}(\rho_M,T)$ and $f^{\text{int}}(\rho_M,T)$ are displayed in Tables 5.2, 5.3 and 5.4. Points along the fluid-BCC coexistence line can be found in Table 5.2 and points along the BCC-FCC/fluid-FCC coexistence line can be found in Table 5.3. In Table 5.4 one can find the defect concentrations for a point outside of the coexistence lines. Values in blue and red indicate respectively that the concentration is calculated in a BCC and an FCC crystal. Looking at these defect concentrations we can observe several interesting things which we will discuss below.

Table 5.2: *Defect concentration along Fluid-BCC coexistence line. Blue text denote a BCC crystal.*

κ	Γ	Crystal	βF^{Perfect}	$\beta\mu^{\text{perfect}}$	βf^{vac}	βf^{int}	$\langle n_{\text{vac}}\rangle$	$\langle n_{\text{int}}\rangle$
2.0	442	BCC	50.6	131.4	-122.3		$1\cdot10^{-4}$	
2.5	708	BCC	31.5	88.8	-80.5	97.5	$2\cdot10^{-4}$	$2\cdot10^{-4}$
3.0	1205	BCC	22.4	66.8	-58.3	75.2	$2\cdot10^{-4}$	$2\cdot10^{-4}$
3.5	2134	BCC	16.8	53.2	-44.9	61.9	$2\cdot10^{-4}$	$2\cdot10^{-4}$
4.0	3950	BCC	13.3	44.4	-36.4	53.1	$3\cdot10^{-4}$	$2\cdot10^{-4}$

Table 5.3: *Defect concentration along BCC-FCC and fluid-FCC coexistence line. Blue and red text denote respectively a BCC and an FCC crystal.*

κ	Γ	Crystal	βF^{Perfect}	$\beta\mu^{\text{perfect}}$	βf^{vac}	βf^{int}	$\langle n_{\text{vac}}\rangle$	$\langle n_{\text{int}}\rangle$
3.0	1720	BCC	30.9	92.9	-79.3	107.7	$1\cdot10^{-6}$	$3\cdot10^{-7}$
		FCC	30.9	92.9	-73.3	109.8	$3\cdot10^{-9}$	$4\cdot10^{-8}$
3.5	2565	BCC	19.7	62.5	-51.9	74.1	$2\cdot10^{-5}$	$9\cdot10^{-6}$
		FCC	19.7	62.4	-47.6	75.8	$3\cdot10^{-7}$	$2\cdot10^{-6}$
4.0	4234	BCC	13.3	46.3	-38.3	57.0	$3\cdot10^{-4}$	$2\cdot10^{-5}$
		FCC	14.2	47.0	-34.7	57.0	$5\cdot10^{-6}$	$4\cdot10^{-5}$
4.5	7483	FCC	11.0	38.1	-27.3	48.6	$2\cdot10^{-5}$	$3\cdot10^{-5}$
5.0	14488	FCC	9.4	33.6	-23.2	44.4	$3\cdot10^{-5}$	$2\cdot10^{-5}$

Table 5.4: *Defect concentration for a point away from the coexistence line. Blue text denote a BCC crystal.*

κ	Γ	Crystal type	β^{Perfect}	$\beta\mu^{\text{perfect}}$	βf^{vac}	βf^{int}	$\langle n_{\text{vac}} \rangle$	$\langle n_{\text{int}} \rangle$
3.0	1300	BCC	24.0	71.7	-62.2		$8.0 \cdot 10^{-5}$	

Coexistence line

As we discussed earlier, the coexistence line we used slightly deviated from the calculated points in Ref. [10]. By comparing the difference in free energy of the BCC and FCC crystal along the phase boundary we can see what the influence of this deviation is on the free-energy difference between the two crystal types. We see that for $\kappa = 3.0$ and $\kappa = 3.5$ the free energy per particle of a perfect crystal is almost the same for FCC and BCC, indicating that these phase points indeed lay on the actual coexistence line. For $\kappa = 4.0$ it turns out that BCC has a lower free energy, meaning that the phase point we used actually lies slightly below the actual coexistence line. However, looking at the snapshots of the particles in an FCC crystal during the simulations we saw that the FCC crystal is at least still meta stable at this point.

Concentration along the Phase Boundary

We see that along all coexistence lines the concentration of vacancies increases when Γ and κ increase. Apparently the combination of an increased interaction energy and an increased screening length increases the value of f^{vac} more than it decreases the value of μ^{vac}, allowing for the forming of more vacancies. For interstitials we do not see the same phenomenon happen. Along the BCC-FCC the concentration of interstitials first strongly increases while going to higher κ. However, when we go to $\kappa \geq 4$ (which is approximately the point where we go from BCC-FCC phase transition to a fluid-FCC phase transition) the concentration starts decreasing. Along the fluid-BCC phase transition it seems like the interstitial concentration just stays constant, however it becomes clear from the not rounded data (not shown here) that actually in this case too the interstitial concentration starts decreasing for $\kappa \geq 3$. For both the fluid-BCC and fluid-FCC phase transition we thus see that, after a certain value of κ, the interstitial concentration decreases.

Concentration of interstitials versus concentration of vacancies

When we compare the interstitial and the vacancy concentrations we see that they are of around the same magnitude; they differ at most by one order of magnitude. Sometimes the concentration of interstitials is even larger than the concentration of vacancies (see for example the point determined by $\kappa = 3.0$ in an FCC crystal). The most striking thing about this result is that it is completely different from the hard sphere case. In that system, as we mentioned in Chapter 1, the interstitial concentration is a factor 10^{-4} lower than the vacancy concentration. This big difference between the two systems may seem surprising, however when one thinks about it a bit more it can make sense. Due to the high energy penalty in the case of overlap in the hard-sphere model, you expect the concentration of interstitials to be quite low in that system. Because the Yukawa system consists of soft-core particles it lacks that high energy penalty due to overlap. Therefore it seems reasonable that the energy cost due to a interstitial is lower, resulting in a higher interstitial concentration.

Concentration dependence on crystal structure

Maybe one of the most striking outcomes is the difference in vacancy concentration between FCC and BCC crystals. Looking at Table 5.3 we see that this concentration at some points differs by a factor of 10^3. Note that this big difference between the two crystals is only there in the case of a vacancy; in the case of interstitials the concentration difference between FCC

and BCC crystals is not that large. The question then of course arises what causes this big difference in vacancy concentration? Because we are at the phase boundary, the value of μ_{perfect} is equal for both crystals, which means that the origin of the difference in concentration needs to lie in the values of f^{vac}. Looking at these free energies we indeed see the values evaluated in the BCC crystal are between 4 and 6 k_BT lower than the corresponding values evaluated in the FCC crystal.

Although there may be many subtle processes that change the value of f^{vac}, the free-energy difference is so big that our first guess is that the geometry of the crystals must have influence (that is after all the main difference between the two crystals). To find the cause for the free energy difference we therefore start by looking at the potential energy in a static crystal, where the particles are not allowed to leave their lattice sites. We compute the potential energy difference between a perfect crystal and a crystal with one vacancy for both the BCC and the FCC crystal. The potential energies we find are:

$$\beta\Delta U_{\text{FCC}}^{\text{static}} = 31.4,$$
$$\beta\Delta U_{\text{FCC}}^{\text{static}} = 31.6.$$

These potential energy differences are almost the same, meaning that they cannot explain the large concentration difference between both crystals. Therefore we look at the same potential energy difference but now in a dynamic crystal, where the particles are now allowed to leave their lattice sites[7]. The new energy differences we find are:

$$\beta\Delta U_{\text{FCC}}^{\text{dynamic}} = 35.6,$$
$$\beta\Delta U_{\text{BCC}}^{\text{dynamic}} = 42.9.$$

In the dynamic case there is definitely a difference in potential energy between the two crystals. Apparently the redistribution of particles in a BCC crystal, due to a vacancy, allows for a larger decrease in potential energy than the redistribution in an FCC crystal. This is a surprising result and therefore it is interesting to take a closer look at how particles redistribute in the presence of a defect, something we will do in the next section.

5.3.2 Crystal structures of systems with a defect

We want to make a quantitative analysis of the particle redistribution due to vacancies to identify differences in the redistribution of particles in BCC and FCC crystals due to a vacancy. Furthermore it is also interesting to look at the redistribution of particles due to an interstitial. Although the concentration differences between the crystals are not big in the case of an interstitial it is still interesting to see how the crystal structure changes due to an interstitial. Before we can take a closer look at the redistribution of particles however, we first need to briefly discuss the geometry of the FCC and BCC crystals and examine the inter-particle distances in both crystals.

FCC and BCC crystals

Both the BCC and the FCC crystal are schematically represented in Figure 2.3. The FCC crystal has unit cells consisting of 4 particles. Each particle has 12 nearest neighbors at a distance $\frac{\sqrt{3}}{2}l_{\text{FCC}}$ with l_{FCC} the lattice constant. In a BCC crystal, a cell unit cell consists of 2 particles. Each particle has 8 nearest neighbors, all at a distance of $\frac{1}{\sqrt{2}}l_{\text{BCC}}$. We want to compare the nearest-neighbor distances of both crystals and therefore we express the lattice constants in terms of the density ρ:

$$l_{\text{FCC}} = \left(\frac{4}{\rho_{\text{FCC}}}\right)^{1/3} \text{ and } l_{\text{BCC}} = \left(\frac{2}{\rho_{\text{BCC}}}\right)^{1/3}. \tag{5.4}$$

[7] However they are still confined to their Wigner Seitz cell.

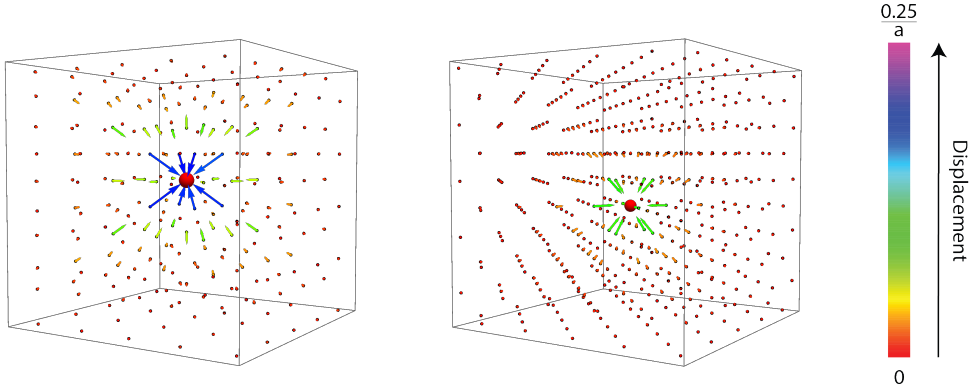

(a) *BCC* (b) *FCC*

Figure 5.7: *Three-dimensional representation of the redistribution of particles due to a vacancy. The red dot indicates the lattice position of the vacancy.*

We can now express the nearest neighbor distances of both crystals in terms of their lattice constants and compare them, however this becomes quite complicated because of the two densities. Fortunately we can simplify things: as discussed in Chapter 2, we express all length in units of the Wigner Seitz radius which means that our system does not depend on either ρ or a. We are thus free to choose the two densities (or rather the two a's) of the two crystals to be the same, making the comparison between the two crystals a lot easier.[8] Using this simplification we can omit all factors of a and show, by using Equation (5.4), that the ratio of nearest neighbor distances is given by:

$$\frac{x^{nn}_{\mathrm{FCC}}}{x^{nn}_{\mathrm{BCC}}} = \frac{\frac{\sqrt{3}}{2} l_{\mathrm{FCC}}}{\frac{1}{\sqrt{2}} l_{\mathrm{BCC}}} = \frac{2^{5/6}}{\sqrt{3}} \approx 1.02.$$

We thus conclude that for the same density the nearest-neighbor distances in an FCC and a BCC crystal have approximately the same value.

Redistribution of particles due to a vacancy

Now that we have discussed the basic geometry of both crystals, we turn our attention to the redistribution of particles due to defects. With the use of simulations we obtain for both crystals the mean particle positions in the presence of a vacancy. To illustrate this displacement graphically, we make a three dimensional plot containing arrows originating from the lattice sites, pointing in the direction of the new particle positions. The three dimensional plots for both the BCC and the FCC crystal are displayed in Figure 5.7: the left figure shows the displacement in a BCC crystal and the right figure shows the displacement in an FCC crystal. These figures are only meant as a qualitative display: the size of the vectors is exaggerated and the length ratio between different vectors is slightly off. However, the colors of the vector do represent the value of the actual displacement. From the three dimensional plot we take the displacement projection on two cross sections parallel to one of the sides of the cube close to the vacancy and plot them on top of each other. In Figure 5.8 we show these cross sections for each of the crystals: the left figure again shows the displacement in a BCC crystal and the right figure shows the displacement in an FCC crystal. In the figures the black and red dots represent the original lattice positions, where the black points indicate the particles laying in the same plane as the vacancy and the red points indicate the particles

[8] When we choose to use different densities, we need to express everything in terms of a, which makes it more complicated to work with. However in the end the analysis is the same.

laying in a neighboring plane. The dotted circle indicates the vacancy lattice site.

From these figures we observe a few interesting things. When we look at the displacement of the nearest and next nearest neighbors it becomes clear that the displacement of particles in an FCC crystal is much smaller than the displacement in a BCC crystals; the ratio of the maximum displacement between both crystals turns out to be a factor of 1/2. We computed earlier that the ratio between nearest neighbor distances in FCC and BCC crystals is approximately one so it really is the case that particles close to the vacancy have a bigger displacement in a BCC crystal than in an FCC crystal.

Another interesting aspect is the exact way the particles redistribute. In the FCC crystal all particles move inward toward the Wigner Seitz cell that 'contains' the vacancy. In the BCC crystal we see that the nearest neighbor particles all move inward too, but the next nearest neighbors move alternately in- and outward. Although it is hard to quantitatively link these results to a decrease in potential energy, it is clear that the two crystals have a completely different particle redistribution. This helps to explain why the vacancy concentrations in the FCC and BCC crystal differ so much from each other.

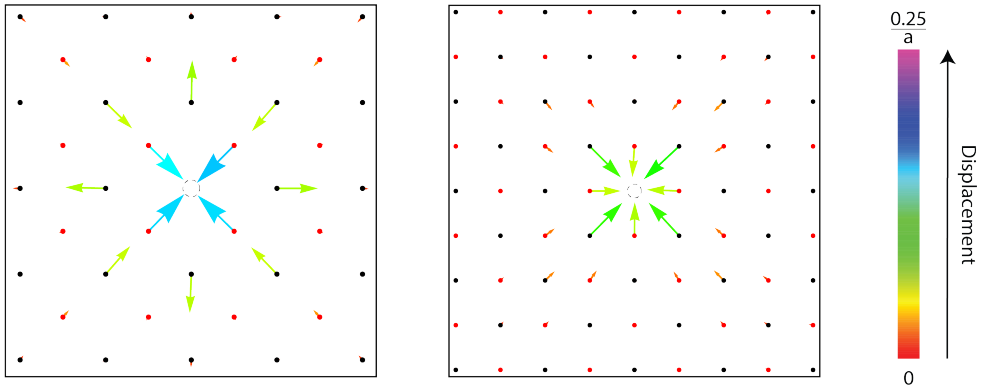

(a) *BCC crystal* (b) *FCC crystal*

Figure 5.8: *Displacement of particles due to a vacancy.*

Redistribution of particles due to an interstitial

As said in the beginning of this section, we are also interested in how the crystal structure changes due to an interstitial. Using the same procedure as in the vacancy case, we obtain the mean displacement of particles from their lattice sites due to the presence of an interstitial. The three dimensional plots that contain the displacement arrows are showed in Figure 5.9: the left figure again shows the displacement in a BCC crystal and the right figure shows the displacement in an FCC crystal. From these figures it becomes clear that in both crystals the distortion is mainly along specific lines; from the perspective of the interstitial, particles laying on the lines going through the nearest neighbors are by far influenced the most. In Figures 5.10 and 5.11 we plot the specific displacement lines schematically for respectively a BCC and an FCC crystal. In the following paragraphs, we will consider the displacement of particles due to an interstitial for each crystal in more detail.

We first take a better look at the redistributions of particles in a BCC crystal. Figure 5.12a displays the displacement along a cross section parallel to one of the sides of the cube (one of the planes displayed in Figure 5.11) and Figure 5.12 displays the displacement along a diagonal cross section (one of the planes displayed in Figure 5.10). Again the length of the

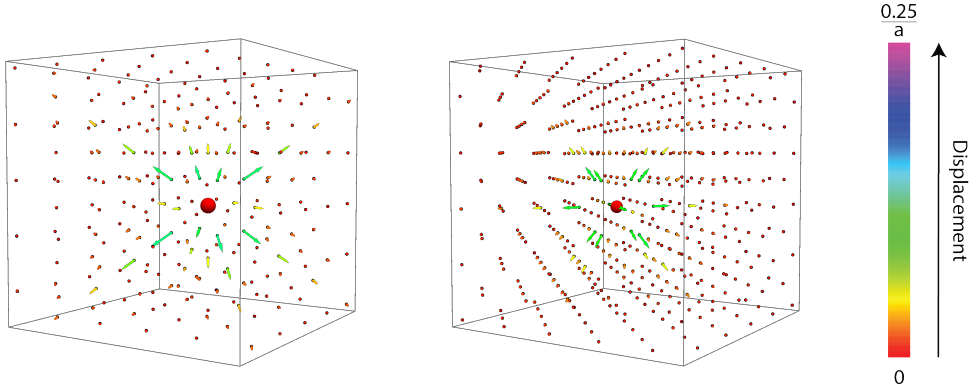

(a) *BCC* (b) *FCC*

Figure 5.9: *Three-dimensional representation of the redistribution of particles due to a interstitial. The red dot indicates the lattice position of the interstitial.*

vectors is exaggerated, but the colors represent the actual displacement. It is clear from these figures that the displacement is foremost along the directions of the nearest neighbors. We also see that the influence of the interstitial reaches quite far, even the particles almost at the edge of the box are displaced slightly[9].

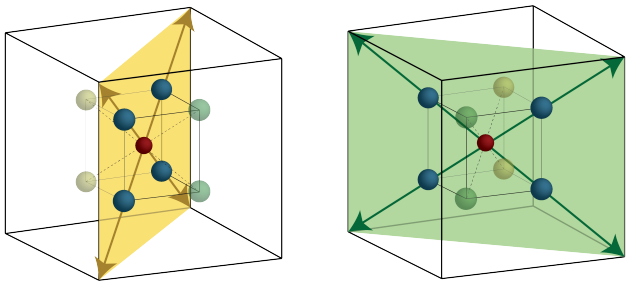

Figure 5.10: *Lines, indicated as arrows, of displacement due to an interstitial in a BCC crystal. The place of the interstitial is indicated as the red dot. The nearest neighbor particles are indicated as the blue, yellow and green particles surrounding the interstitial.*

Finally we take a better look at the displacement of particles in an FCC crystal due to an interstitial. In Figure 5.13 we display a cross-section of this three dimensional representation parallel to one of the sides of the cube (one of the planes displayed in Figure 5.11). Again the influence of the interstitial stretches quite far along the displacement lines. When we compare Figure 5.13 with Figure 5.12b, we can conclude that the planes, except for the fact the orientation of the plane itself is different, look quite the same. The fact that the displacement looks the same in both crystals could explain why the interstitial concentrations in both systems are quite similar. However, although the figures look the same, there are also some small but potentially very important differences between the two crystals.

[9]Note that because of periodic boundary conditions the particles at the edge of the box feel both the real interstitial as well as the periodic image of it with almost equally. This means that the real influence of the interstitial at the particles close to the boundary is hard to tell. We will come back to this later.

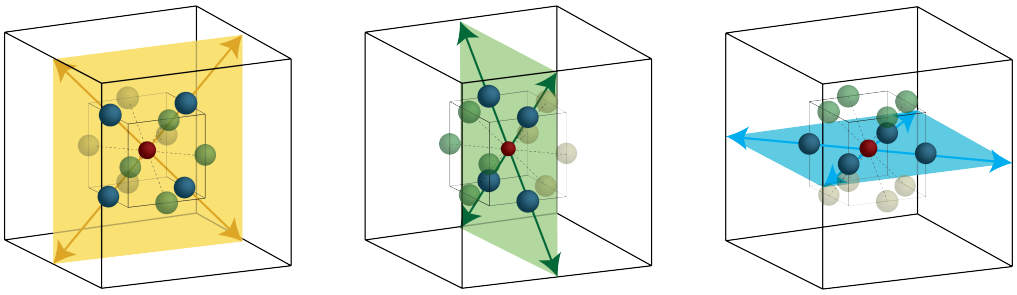

Figure 5.11: *Lines, indicated as arrows, of displacement due to an interstitial in an FCC crystal. The place of the interstitial is indicated as the red dot. The nearest neighbor particles are indicated as the blue, yellow and green particles surrounding the interstitial.*

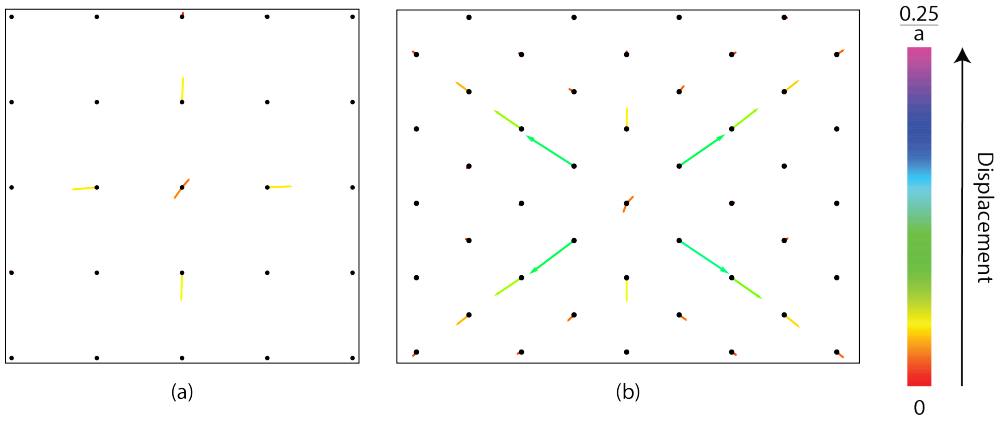

Figure 5.12: *Displacement of particles due to an interstitial in a BCC crystal. The left figure contains particles laying in one of the planes indicated in Figure 5.10, the right figure contains particles laying in one of the planes indicated in Figure 5.11. The actual length of vectors is indicated by their color.*

First of all we see that, compared to the FCC case, in the BCC crystal the interstitial pushes particles further outwards[10]. Note however, as said earlier, that it is not possible to say something about how far the influence of the interstitial really stretches, because the particles at the edge of the system feel both the real interstitial as well as its periodic image with approximately the same strength. To solve this problem we would have to look at larger systems which was not possible in the time frame of this project. Another difference between both crystals is the mean displacement of the particles associated with the interstitial (so the two particles that are in the same Wigner Seitz cell). In the FCC crystal these mean displacements are very small, almost negligible. However, in the BCC crystal these displacements clearly have a non-zero length. This non zero displacement might seem as pure coincidence, due to a spread in statistics. However we think something else might be causing it and we will take a closer look at it in the next section.

[10] We can see this by looking at the colors of the the displacement vectors.

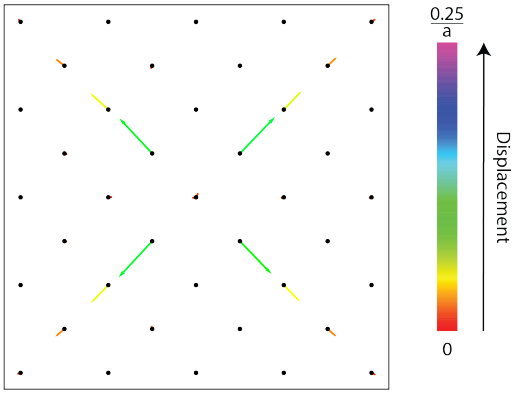

Figure 5.13: *Displacement of particles in an FCC crystal due to a vacancy. The figure contains particles laying in one of the planes indicated in Figure 5.11. The actual length of vectors is indicated by their color.*

Crowdions

As a warning this section is somewhat hypothetical; more research is needed to make firm claims. However we still discuss it because the current results are already quite interesting. Our hypothesis is that in the BCC case, instead of the interstitial pushing out particles simultaneously in all nearest neighbor directions (as most likely happens in the case in the FCC crystal), a crowdion forms.

In Chapter 1 we already briefly mentioned crowdions as extended one-dimensional distortions of the crystal lattice due to an interstitial in the 111 direction [7]. The four possible 111 directions are precisely indicated by the arrows in Figure 5.11 and it is thus clear that in a BCC crystal the main particle displacements due to an interstitial are along these 111 directions. However the important characteristic of crowdions is that they are one dimensional. With this we mean that the distortion is in only one of the 111 directions at a time, leaving the rest the crystal almost unaffected.

The fact that the mean displacement of the particles associated with the interstitial in the BCC crystal is non-negligible might indicate the presence of crowdions. After all it could mean that the system has spent more time in one of the 111 directions than in the others, resulting in a non-zero mean displacement. However it is not possible to draw any further conclusions by only looking at the mean particle displacements over a long time interval. Even if there would be a crowdion present, the system would almost certainly have switched multiple times between different 111 directions after running for a long time, making it look like the displacement of particles is in all four directions simultaneously. We therefore look at mean displacements during smaller time intervals. Although this means that you have less statistics and thus a bigger error in the displacements, it still seemed the case that for many of the time intervals the main displacement of particles was only in one of the 111 directions.[11] As said earlier, we cannot end this section with any decisive conclusions to whether crowdions form in our BCC crystal or not, however the results mentioned above do indicate that it is indeed interesting to take an even closer look at the behavior of interstitials in BCC crystals of point Yukawa particles in the future.

[11] We will not include these figures because we cannot draw any real conclusions from them due to the fact that they are based on too little statistics.

Chapter 6

Conclusions & Outlook

In this thesis we investigated the concentration of vacancies and interstitials along several points of the fluid-BCC and BCC-FCC/fluid-FCC coexistence line in a crystal with soft-core Yukawa particles. Furthermore we looked at how defects change the crystalline structure. We found that along the fluid-BCC phase boundary both the vacancy and interstitial concentrations are of the order 10^{-4}. Along the BCC-FCC/fluid-BCC boundary the concentrations in the BCC crystal lies between 10^{-4} and 10^{-6}, while in the FCC crystal the concentration lies between 10^{-9} and 10^{-5}. Although we now have quite a good picture of the concentration of defects in the Yukawa system, we did not consider very long range interaction regimes ($\kappa \leq 2$). In the future this regime also needs to be studied. We are aware of the fact that the for higher κ's the phase points we used turned out to be slightly away from the real coexistence line. However because the crystals we looked at were still metastable the results we obtained still give a good indication of the defect concentrations of the crystals.

From the outcomes of the concentration calculations we could draw several conclusions. First of all we conclude that the concentration of vacancies and interstitials is almost on the same order of magnitude. This outcome is very different from the archetypical hard-sphere case where the concentration difference between both defects is on the order of 10^4 [4]. Furthermore it became clear that the type of crystal has a very large influence on the vacancy concentration along the phase boundary; for some phase points the concentration in the BCC crystal was about 10^3 times higher than the concentration in the FCC crystal. We found that this large concentration difference is due to the distinctive redistribution of particles in the presence of a vacancy. In the case of a BCC crystal this redistribution allows for a larger decrease in potential energy than in the case of an FCC crystal, resulting in a higher vacancy concentration.

We also looked at how an interstitial influenced the redistribution of particles. It turned out that in both types of crystal it causes a distortion along the directions of the nearest neighbors. Especially in the BCC crystal this distortion effects the particles along these lines up to quite a large distance[1]. Although after running the simulation for a long time the mean displacement of particles in both crystals looked approximately the same, we suspect that when we look at smaller time intervals the displacement might look different in both crystals. Our hypothesis is that, similar to the system discussed in Ref. [7], crowdions form in the BCC crystal. If this is the case the distortion due to the interstitial is one-dimensional, meaning that it exists only along one of the 111 direction at a time instead of along all four 111 directions simultaneously. This hypothesis is supported by the fact that when we look at smaller time intervals it seems like the distortion occurs only along one of the 111 directions. Another indication that crowdions are forming is the fact that, contrary to the FCC crystal, the mean displacement of the particles associated with the interstitial is negligible. Although the phenomena we looked at support the crowdion hypothesis, we cannot draw any firm conclusions yet, due to the limited scope of these first series of simulations. However because

[1] We cannot say exactly how far the distortion extends due to the small size of our system

the possibility of the formation of crowdions in a BCC crystal of point Yukawa particles is very interesting we will conduct more research in the future to give a definitive answer to whether crowdions really exist in this system. To do this we first need the modeled system to be bigger, because we need to see how far the influence of the interstitial really stretches. Furthermore we need to look at the distortion of the particle positions in the system as a function of time to see whether this distortion really is one-dimensional. Of course these results need to be compared with the FCC crystal to see whether the phenomena are really different from each other.

Another conclusion we can draw from this thesis is that in these types of systems, Wang Landau biasing does not perform well. Although this method in general is very useful it does not work in systems where the energy of the system fluctuate heavily for constant order parameters .

Chapter 7

Acknowledgments

During the work on this thesis a lot of people have helped and supported me and I would like to take the time to thank them. First of all there is of course my supervisor Laura Filion, whose guidance and affirmation throughout the entire project were of great importance to me. Furthermore she took a lot of time to sit with me and discuss how to write things down clearly, something from which I learned a lot. Berend van der Meer was also a great support. After a soft knock on the door, he had always time to discuss simulations and results. Besides the discussions, Berend also helped me a lot by simulating simulations along mine, which made it possible to check my own code.

I also would like to thank Jillis Schokking, with whom I worked together for the first few weeks. He helped me a lot with learning how to code. The other person I worked with a lot, although not on the same project, was Laura Ackermans. We've spent many Fridays working at the kitchen table with an occasionally well deserved climbing break. I also want to thank her for giving feedback on some parts of my thesis.

Next I want to thank my family; my father who read some of the earlier versions and my mother and sister, who (almost ;) always listened enthusiastically to my stories about colloidal systems and Monte Carlo simulations.

And last but not least I want to thank all the students in the student room for all the lunches in the Minneart building, the coffee breaks and the hilarious conversations.

Bibliography

[1] A. M. Russel and L. L. Russell, Structure-property relations in nonferrous metals (John Wiley and Sons, Ltd, 2005).

[2] W. F. Smith and J. Hashemi, Foundations of material science and engineering (McGraw-Hill, 2001).

[3] C. H. Bennett and B. J. Alder, Studies in molecular dynamics. IX. vacancies in hard sphere crystals, J. Phys. Chem. B **54**, 4796 (1971).

[4] S. Pronk and D. Frenkel, Point defects in hard-sphere crystals, J. Phys. Chem. B **105**, 6722 (2001).

[5] W. Lechner and C. Dellago, Defect interactions in two-dimensional colloidal crystals: vacancy and interstitial strings, Soft Matter **5**, 2752 (2009).

[6] B. van der Meer, Ph.D. thesis, Utrecht University, 2018.

[7] P. M. Derlet, S. L. D. Nguyen-Manh, and Dudarev, Multiscale modeling of crowdion and vacancy defects in body-centered-cubic transition metals, Phys. Rev. B , 054107 (2007).

[8] A. Hynninen, Ph.D. thesis, Utrecht University, 2005.

[9] P. Hopkins, A. J. Archer, and R. Evans, Pair-correlation functions and phase separation in a two-component point Yukawa fluid, J. Chem. Phys. **124**, 054503 (2006).

[10] S. Hamaguchi, R. T. Farouki, and D. H. E. Dubin, Triple point of Yukawa systems, Phys. Rev. E **56**, 4671 (1997).

[11] A. Hynninen and M. Dijkstra, Phase diagram of hard-core repulsive Yukawa particles with a density-dependent truncation: a simple model for charged colloids, J. Phys. Condens. Matter **15**, S3557 (2003).

[12] D. Frenkel and B. Smit, Understanding molecular simulation (Academic Press, Inc., 2001).

[13] D. Frenkel, Simulations: The dark side, Eur. Phys. J. Plus **128**, (2012).

[14] E. B. Kim, R. Faller, Q. Yan, N. L. . Abbott, and J. J. de Pablo, Potential of mean force between a spherical particle suspended in a nematic liquid crystal and a substrate, J. Chem. Phys. **117**, 7781 (2002).

[15] J. M. Polson, E. Trizac, S. Pronk, and D. Frenkel, Finite-size corrections to the free energies of crystalline solids, J. Chem. Phys. **112**, 5339 (2000).

[16] E. de Miguel and G. Jackson, The nature of the calculation of the pressure in molecular simulations of continuous models from volume perturbations, J. Chem. Phys. **125**, 164109 (2006).

[17] R. J. Speedy, Pressure and entropy of hard-sphere crystals, J. Phys. Condens. Matter **10**, 4387 (1998).

[18] N. E. Carnahan and K. E. Starling, Equation of state for nonattracting rigid spheres, J. Chem. Phys. **51**, 635 (1969).

Appendix A

NPT and *NVT* ensemble

For the simulations in this thesis we need a working Monte Carlo simulation of an NVT ensemble. To check whether this simulation works correctly, we do an NPT Monte Carlo simulation of hard spheres with a potential

$$\phi(r) = \begin{cases} 0 & \text{if r } > \sigma, \\ \infty & \text{if r } \leq \sigma, \end{cases}$$

with σ the particle diameter. Because the simulation of an NPT ensemble has an NVT-ensemble embedded in it, verifying that our NPT code works, also verifies that we have a working NVT ensemble. To check the simulation, we compare the simulated equilibrium density for a given value of the pressure, βP, with the theoretical density.

Theory

The phase diagram of hard spheres consists of a fluid and an FCC phase. For hard spheres in an FCC configuration, the equation of state is well approximated by [17]

$$\frac{PV}{Nk_BT} = \frac{3}{1-z} - \frac{a(z-b)}{z-c}, \tag{A.1}$$

with P the pressure, V the volume, N the number of particles, k_B the Boltzmann constant, T the temperature, $z = (N/V)\sigma^3/\sqrt{2}$, $a = 0.5921$, $b = 0.7072$ and $c = 0.601$.

For hard spheres in a fluid phase the equation of state is well approximated by the Carnahan-Starling Equation [18]:

$$\frac{PV}{Nk_BT} = \frac{1+\eta+\eta^2-\eta^3}{(1-\eta)^3}, \tag{A.2}$$

with η the packing fraction.

The program is run multiple times for different values of $\beta P\sigma^3$. Around $\beta P\sigma^3 \approx 11$ a phase transition occurs between a fluid and an FCC crystal and it depends on the initial configuration whether the simulation will result in a fluid or an FCC crystal. Therefore around $\beta P\sigma^3 = 11$ the program uses both fluid and crystal initial configurations. In Figure A.1 we plot the values obtained for $\beta P\sigma^3$ for different values of $\rho\sigma^3$, together with the theoretical equations of state given by Equations (A.1) and (A.2). Clearly, from Figure A.1, we find excellent agreement between the approximations and our simulations. Hence we conclude we have a working NPT simulation.

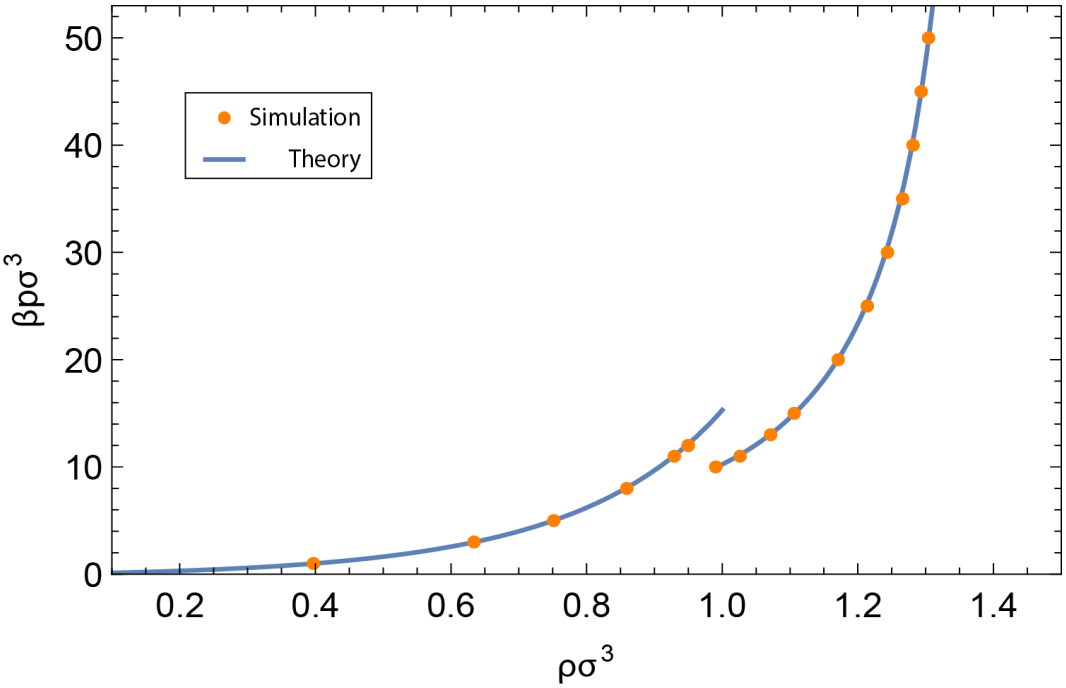

Figure A.1: *Equation of state for hard spheres. Blue lines indicate the theoretical Equations of state* (A.1) *and* (A.2)*. Orange dots indicate data acquired by simulations.*

Appendix B

Yukawa crystal

To check the simulation of a soft-core Yukawa crystal, we compute a quantity quite similar to the potential energy in our system and compare it with the data given in the paper of Hamaguchi, Fraouki and Dubin (1997) [10]. The quantity we look at is defined by:

$$\frac{U}{Nk_BT} = \Gamma \left[\frac{1}{N} \sum_{j=1}^{N-1} \sum_{k=j+1}^{N} \mathbf{\Phi}\left(\frac{\mathbf{r}_{jk}}{a}\right) - \frac{3}{2\kappa^2} - \frac{\kappa}{2} \right], \tag{B.1}$$

where $\mathbf{\Phi}(\mathbf{r})$ is given by $4\pi\epsilon_0 a\phi(\mathbf{r})/Q^2$, with $\phi(\mathbf{r})$ defined in Equation (2.2) and where $\mathbf{r}_{ij}$ is the distance between particles i and j. Equation (B.1) can be rewritten as:

$$\frac{U}{Nk_BT} = \Gamma \left[\frac{1}{N} \sum_{j=1}^{N-1} \sum_{k=j+1}^{N} \Gamma\left(\frac{a}{\mathbf{r}_{jk}}\right) \exp[-\kappa\left(\frac{a}{\mathbf{r}_{jk}}\right)] - \frac{3}{2\kappa^2} - \frac{\kappa}{2} \right], \tag{B.2}$$

We compute Equation (B.2) for both the FCC and BCC crystal at the phase point determined by $\kappa = 4.0$ and $\Gamma = 13.000$. For our system we use the truncation of the potential as discussed in Section 4, however for the data in the paper it is not clear what sort of truncation is used. According to the paper the values should be:

$$\left.\frac{U_{FCC}}{k_BTN\Gamma}\right|_{\kappa=4.0,\Gamma=13000} = -2.091193 \pm 0.000004$$
$$\left.\frac{U_{BCC}}{k_BTN\Gamma}\right|_{\kappa=4.0,\Gamma=13000} = -2.091169 \pm 0.000003$$

In our simulations we find

$$\left.\frac{U_{FCC}}{k_BTN\Gamma}\right|_{\kappa=4.0,\Gamma=13000} = -2.091193 \pm 0.000006$$
$$\left.\frac{U_{BCC}}{k_BTN\Gamma}\right|_{\kappa=4.0,\Gamma=13000} = -2.091230 \pm 0.000006$$

For the FCC crystal the two results are the same up to the used precision, while in the BCC case the numbers, although quite similar, differ more than the range of the error bars. Given the fact, however, that the truncation that is used in the simulations of the paper is unknown, such a small difference as we see in the FCC case could be expected. Hence we can conclude that the simulation of our crystal with Yukawa particles works correctly.

Appendix C

Wang Landau biasing

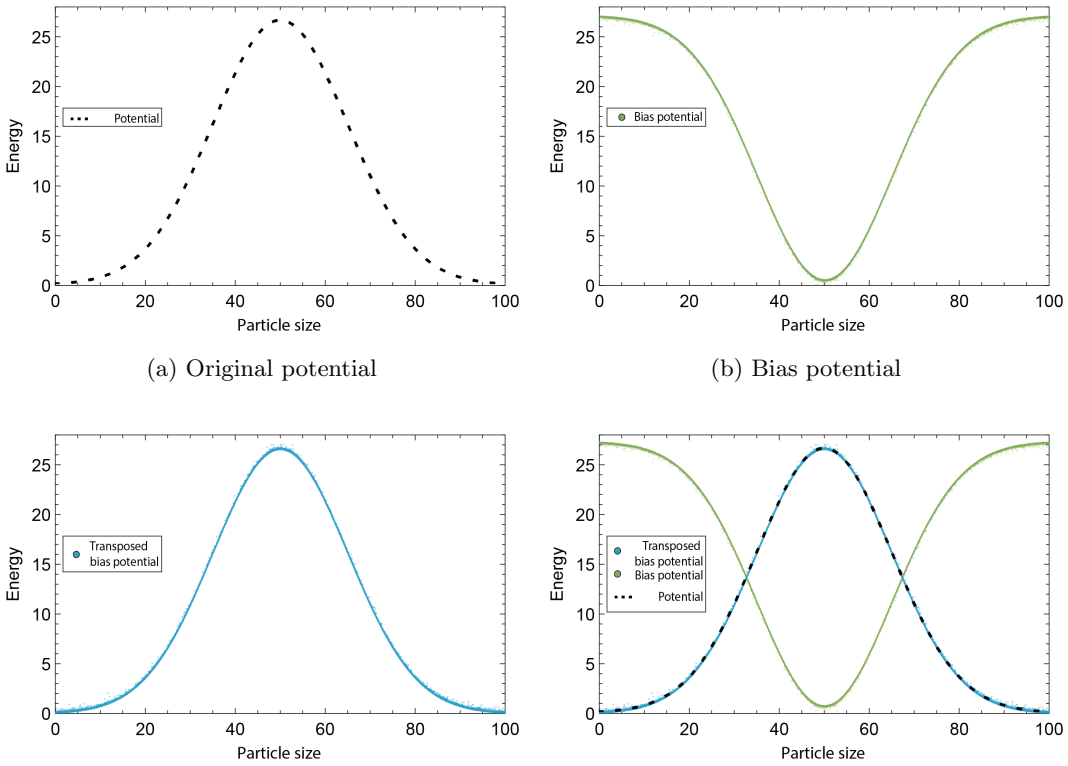

(a) Original potential

(b) Bias potential

(c) Transposed bias potential

(d) Figures (a), (b) and (c) plotted together

Figure C.1: Check of the Wang Landau biasing potential.

To see if our Wang Landau biasing simulation works correctly, we test it by biasing a system where we know the original potential in advance. If the biased potential and the original potential together form a uniform distribution, we can conclude that our biasing code works correctly.

In our case we look at a system of one particle that has a variable size. The order parameter is in this system represented by the radius r of the particle, where we let the radius can fluctuate between 0 and 100. The potential we impose on the system depends only on the radius of the particle and has the shape of a uniform distribution,

$$\phi(r) = \frac{1000}{\sqrt{2\pi 15^2}} e^{-\frac{(r-50)^2}{2\cdot 15^2}}.$$

We run the program with an initial g of 1 and let the initialization loops run until $g < 10^{-6}$. If the bias potential and original potential together indeed form a uniform distribution, we can use geometry to show that the following must be true: the biased potential, mirrored in the horizontal line through the intersections of the two potentials, must overlap with the original potential perfectly. In Figures C.1a, C.1b, C.1c we plot respectively the original potential, the biased potential and the transposed bias potential separately and in Figure C.1d we plot all three together. It is clear from this figure that the bias potential indeed overlaps perfectly with the original potential and therefore we may conclude that our Wang Landau biasing works correctly.